Netrin-1 feedforward mechanism promotes pancreatic cancer liver metastasis via hepatic stellate cell activation, retinoid, and ELF3 signaling

Crissy Dudgeon, Anthony Casabianca, Chris Harris, Charline Ogier, Mélanie Bellina, Stephany Fiore, Agnes Bernet, Benjamin Ducarouge, David Goldschneider, Xiaoyang Su, et al.

Cell Reports

Article

Netrin-1 feedforward mechanism promotes pancreatic cancer liver metastasis via hepatic stellate cell activation, retinoid, and ELF3 signaling

Graphical abstract

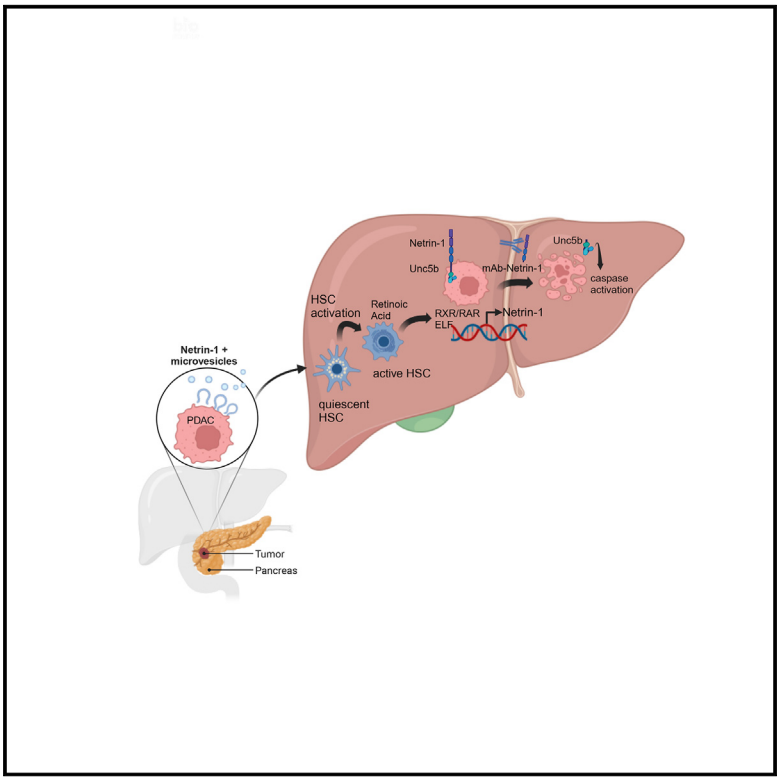

Authors

Crissy Dudgeon, Anthony Casabianca, Chris Harris, ..., Igor Astsaturov, Patrick Mehlen, Darren R. Carpizo

Correspondence

darren_carpizo@urmc.rochester.edu

In brief

Therapeutic strategies that target the unique biology of metastatic pancreatic cancer are needed. Netrin-1, an embryonic axon guidance molecule, is upregulated in pancreatic liver metastases through a mechanism involving hepatic stellate cell-secreted retinoic acid. Targeting Netrin-1 inhibits metastasis and improves survival in murine pancreatic cancer models.

Highlights

- Netrin-1 is upregulated in metastatic pancreatic cancer
- Hepatic stellate cell-secreted retinoic acid upregulates Netrin-1 in the liver
- Netrin-1 on extracellular vesicles pre-conditions the metastatic niche
- Anti-Netrin-1 therapy inhibits metastasis and improves survival in murine PDAC

Dudgeon et al., 2023, Cell Reports *42*, 113369
November 28, 2023
https://doi.org/10.1016/j.celrep.2023.113369

CellPress

Cell Reports

CellPress
OPEN ACCESS

Article

Netrin-1 feedforward mechanism promotes pancreatic cancer liver metastasis via hepatic stellate cell activation, retinoid, and ELF3 signaling

Crissy Dudgeon,[1,11] Anthony Casabianca,[2,3,11] Chris Harris,[2,3,11] Charline Ogier,[4] Mélanie Bellina,[5,6] Stephany Fiore,[5] Agnes Bernet,[5,6] Benjamin Ducarouge,[6] David Goldschneider,[6] Xiaoyang Su,[1] Jason Pitarresi,[8] Aram Hezel,[7] Subhajyoti De,[1] Wade Narrow,[2,3] Fady Soliman,[9] Cory Shields,[3] Debora Barbosa Vendramini-Costa,[4] Orjola Prela,[2] Lan Wang,[10] Igor Astsaturov,[4] Patrick Mehlen,[5,6] and Darren R. Carpizo[2,3,12,*]

[1]Rutgers Cancer Institute of New Jersey, New Brunswick, NJ, USA
[2]Department of Surgery, Division of Surgical Oncology, University of Rochester School of Medicine and Dentistry, Rochester, NY, USA
[3]Wilmot Cancer Center, University of Rochester, Rochester, NY, USA
[4]Department of Medical Oncology, Fox Chase Cancer Center, Philadelphia, PA, USA
[5]Apoptosis, Cancer and Development Laboratory - Equipe labellisée "La Ligue," LabEx DEVweCAN, Institut Convergence PLAsCAN, Centre de Recherche en Cancérologie de Lyon (CRCL), INSERM U1052-CNRS UMR5286, Université de Lyon, Université Claude Bernard Lyon 1, Centre Léon Bérard, 69008 Lyon, France
[6]Netris Pharma, 69008 Lyon, France
[7]Department of Medicine, Division of Medical Oncology, University of Rochester School of Medicine and Dentistry, Rochester, NY, USA
[8]Department of Medicine, Division of Hematology/Oncology, University of Massachusetts, Worcester, MA, USA
[9]Rutgers Robert Wood-Johnson Medical School, New Brunswick, NJ, USA
[10]Department of Pathology and Laboratory Medicine, University of Rochester School of Medicine and Dentistry, Rochester, NY, USA
[11]These authors contributed equally
[12]Lead contact
*Correspondence: darren_carpizo@urmc.rochester.edu
https://doi.org/10.1016/j.celrep.2023.113369

SUMMARY

The biology of metastatic pancreatic ductal adenocarcinoma (PDAC) is distinct from that of the primary tumor due to changes in cell plasticity governed by a distinct transcriptome. Therapeutic strategies that target this distinct biology are needed. We detect an upregulation of the neuronal axon guidance molecule Netrin-1 in PDAC liver metastases that signals through its dependence receptor (DR), uncoordinated-5b (Unc5b), to facilitate metastasis *in vitro* and *in vivo*. The mechanism of Netrin-1 induction involves a feedforward loop whereby Netrin-1 on the surface of PDAC-secreted extracellular vesicles prepares the metastatic niche by inducing hepatic stellate cell activation and retinoic acid secretion that in turn upregulates Netrin-1 in disseminated tumor cells via RAR/RXR and Elf3 signaling. While this mechanism promotes PDAC liver metastasis, it also identifies a therapeutic vulnerability, as it can be targeted using anti-Netrin-1 therapy to inhibit metastasis using the Unc5b DR cell death mechanism.

INTRODUCTION

One of the defining features of pancreatic adenocarcinoma (PDAC) is its proclivity for early metastatic dissemination. This is underscored by two facts: (1) the majority of patients (85%) are stage IV at diagnosis; and (2) the overwhelming majority (>80%) of patients with early-stage resectable disease succumb to metastatic recurrence. This highlights the need to better understand the biology of metastatic PDAC to identify therapeutic targets. Recent studies have found that metastatic pancreatic cancer is driven more by global epigenetic reprogramming than by metastasis-specific gene mutations, with some exceptions such as parathyroid hormone-related protein.[1,2] This reprogramming leads to the selection of genetic programs that confer survival for disseminated tumor cells. One such category in advanced PDAC is that of axonal guidance genes, which include members of four canonical families (netrins, semaphorins, slits, and ephrins).[3] These gene families were originally described for their involvement in neuronal development but have recently been implicated in cancer biology, particularly the later stages of tumor progression and metastasis.[4]

Netrin-1 is a secreted, laminin-like protein that was initially described for its role as both an axon attractant and repellent across a diverse number of organisms.[5,6] The Netrin-1 receptors DCC (deleted in colon cancer) and uncoordinated-5 (Unc5; in mammals there are four: Unc5a, Unc5b, Unc5c, Unc5d) belong to the family of dependence receptors (DRs) that mediate different functions depending on whether they are ligand bound or unbound.[7] In the presence of ligand, cells receive positive signals (survival, proliferation, migration) while in the absence of ligand, cells receive negative signals (apoptosis).[4] Through their death-inducing pathway, DRs function as tumor suppressors

with three described means of inactivating this pathway for tumor progression and metastasis: (1) upregulation of the ligand (i.e., Netrin-1); (2) loss of expression of its receptor (through loss of heterozygosity or epigenetic silencing); and (3) loss of downstream death signaling partners.[4,8] In metastasis, upregulation of Netrin-1 in breast cancer has been reported as a survival mechanism, although the mechanism of this upregulation is unknown.[9]

While Netrin-1 has been found to be upregulated in PDAC,[10] its role in PDAC tumor progression is poorly understood. Here we describe that Netrin-1 becomes upregulated to drive PDAC metastasis through the DR Unc5b. For the first time we show that Netrin-1 is detected on the surface of extracellular vesicles (EVs), which function to facilitate liver metastasis through the activation of hepatic stellate cells (HSCs). The mechanism of Netrin-1 upregulation in disseminated tumor cells is mediated by a feedforward mechanism whereby EVs containing Netrin-1 activate HSCs to secrete retinoic acid, which upregulates Netrin-1 by both RAR/RXR- and Elf3-mediated mechanisms. Disruption of Netrin-1/Unc5b signaling both genetically and pharmacologically prevents metastasis and increases survival in murine and human PDAC models, validating Netrin-1 as a therapeutic target for metastatic PDAC.

RESULTS

Netrin-1 is upregulated in metastatic PDAC

We identified Netrin-1 as a gene upregulated in metastatic tumors from a murine PDAC model (INK4.1^{syn_Luc}) whereby immunocompetent FVB mice were orthotopically injected with a primary pancreatic cancer cell line (Ink4a.1) derived from the Pdx-1-Cre;Kras$^{G12D/+}$;p16$^{-/-}$;p19$^{-/-}$ murine model.[11,12] This spontaneously disseminating model was used to harvest liver and peritoneal metastases for RNA sequencing (RNA-seq) and cell-line establishment. When we compared the liver metastases to the primary tumors in this model, we observed marked differences in morphology. The histology of the primary tumors was poorly differentiated, with scattered glandular-appearing cells consistent with the quasi-mesenchymal subtype that this cell line was previously classified[13] (Figure 1Ai). E-cadherin staining of primary tumors exhibited a lack of staining in the mesenchymal-like tumor cells and positive staining in the well-differentiated cells which were sparse (Figure 1Aii). Collagen deposition was observed at the stromal border along the tumor edge (Figure 1Aiii), similar to other orthotopic models of pancreatic cancer.[14–16] While the primary tumors resembled the quasi-mesenchymal subtype of pancreatic cancer, liver metastases displayed hallmarks consistent with the "classic" molecular subtype of pancreatic cancer, including well-differentiated areas with more tumor cells forming glandular structures (Figure 1Aiv) with high expression of E-cadherin (Figure 1Av) and robust collagen stroma (Figure 1Avi).

We hypothesized that the observed plasticity in morphology in the metastatic tumors is a consequence of epigenetic reprogramming. We compared the transcriptomes from metastatic and primary tumor tissue (n = 5 for both) by total RNA-seq and found the transcriptomes to be substantially different, as evident from the volcano plot showing p value and fold change of gene expression between groups (Figure S1A). We then examined a cell line derived from a liver metastasis (Met38) for differential open chromatin regions in comparison to the parental cells using the assay for transposase accessible chromatin (ATAC-seq). While genome-wide higher-order chromatin accessibility patterns were largely comparable (see example of chromosome 1, Figure S1B), a total of 238 loci showed significant changes in chromatin accessibility. The primary tumor cell line, Ink4a.1, had 51 regions of open chromatin that were not observed in the metastatic line, Met38, whereas the latter had gain of open chromatin in 187 regions (Figure S1C). Taken together, these data indicate that this model recapitulates the cellular plasticity characteristic of epithelial-to-mesenchymal transition (EMT) and mesenchymal-to-epithelial transition (MET) in human metastatic biology.[17,18]

We performed a differential gene expression analysis comparing hepatic metastases to primary tumors. Pathway enrichment analysis for Biological Processes showed top upregulated pathways included Developmental Biology, Nervous System Development, Axon Guidance, Extracellular Matrix Organization, Regulation of IGF uptake, and Signaling by PDGF (Figures 1B [left] and S1D [left]). Top downregulated enriched pathways include Cell-Cell Signaling, Biological and Cellular Adhesion, Small Molecule Biosynthetics Process, and Epithelial Cell Differentiation (Figures 1B [right] and S1D [right]). Taken together, these pathways have been shown by others as part of the metastatic process for pancreatic cancer.[19–22] Differential gene expression involved in pancreatic cancer metastasis included upregulation of *Pdgfrb*[23] and *Cldn9* (and downregulation of *Cldn1*[24]). Interestingly, metastatic tumors were high in Col6a3 (type VI collagen), which has previously been shown to be highly expressed in human PDAC as part of the desmoplastic stroma,[25] consistent with what we observed morphologically (Figure 1Avi). We also observed that Netrin-1 was among the most upregulated genes (Figure 1B). Previous reports have shown expression of multiple axon guidance genes in PDAC, including Slit, Robo, and Sema3, and their importance regulating perineural invasion, a common feature of PDAC.[3,26–28] Homing in on the expression of this pathway from our dataset shows that *Ntn1* was the most upregulated (Figure 1B, bottom). We validated this result on a small subset of these genes by quantitative PCR (qPCR) using four cell lines derived from separate hepatic metastases (Met25, Met35, Met36, and Met38). Compared to the parental Ink4a.1 cell line, *Ntn1*, *Selp*, and *Pdgfb* were all significantly upregulated while expression of *Basp1* trended downward, validating the RNA-seq results (Figure S1E). To confirm this result at the protein level, we examined Netrin-1 expression by immunohistochemistry of primary and metastatic tumor tissue. We found greater Netrin-1 expression in hepatic metastasis compared to primary tumors in the orthotopic model (Figure S1F). We created primary cell lines from several metastatic liver tumors and found Netrin-1 to be upregulated when compared to the Ink4a.1 primary tumor cell line (Figure 1C). To validate this in human PDAC, we performed Netrin-1 immunohistochemical staining on a tissue microarray (TMA) composed of 93 PDAC samples containing 18 metastatic and 75 primary tumors and found that Netrin-1 was significantly greater in the metastatic tumors ($p = 0.03$) (Figure 1D). We found a similar result in a separate TMA composed of 25 PDAC specimens taken from patients with stage II primary cancers and stage IV metastatic disease where Netrin-1 was greatest in metastatic tumors (Figure S1G). Owing

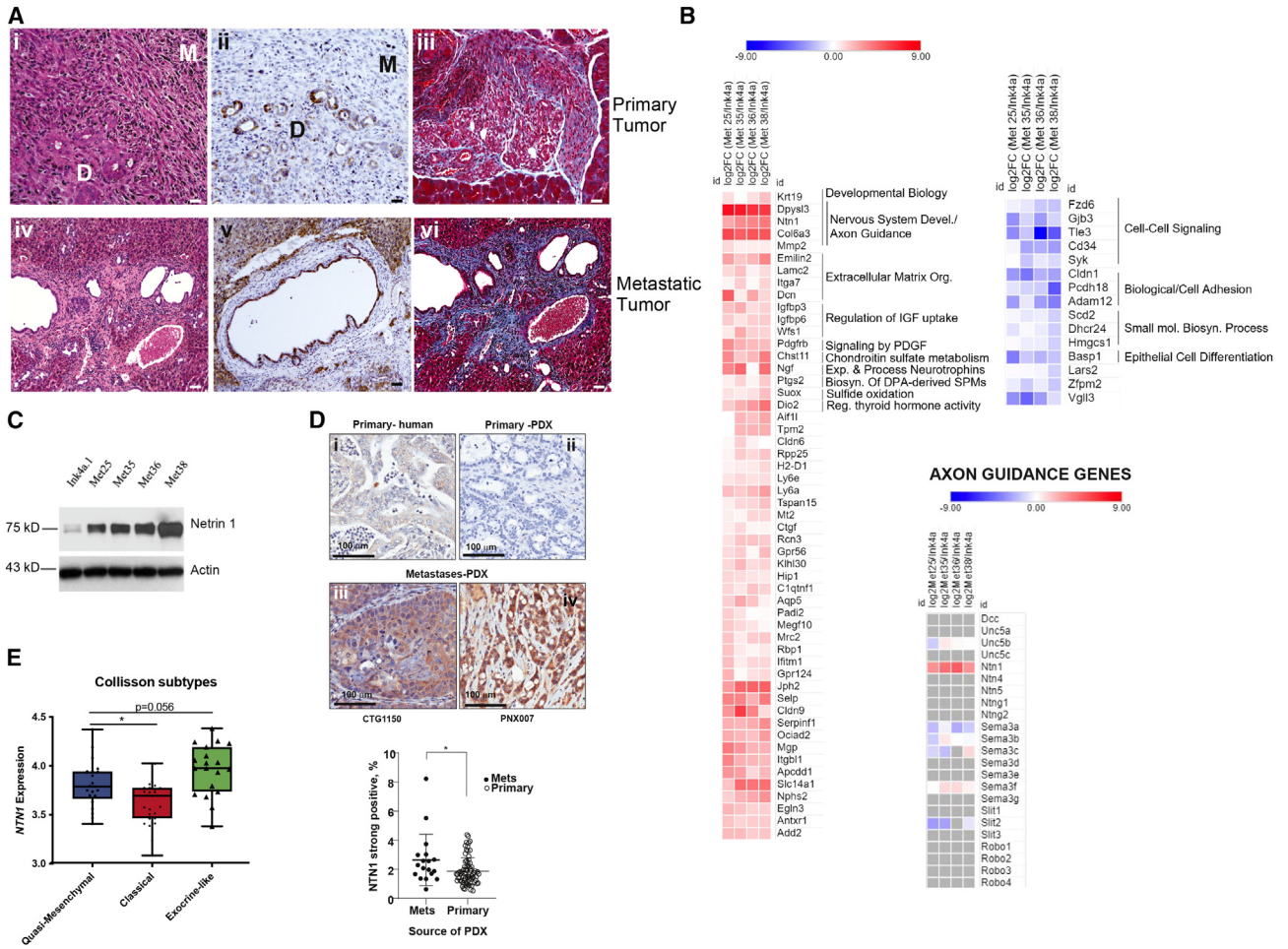

Figure 1. Netrin-1 is upregulated in metastatic PDAC

(A) Histology of a representative primary and metastatic pancreatic tumor to the liver displaying both mesenchymal (M) and epithelial (well-differentiated) features (D). H&E (i, iv), E-cadherin (ii, v), Masson's trichrome (iii, vi) staining. Scale bars, 50 μm (i, ii) and 100 μm (iii–vi).

(B) Heatmaps of overexpressed (left) and underexpressed (right) genes as well as the axon guidance gene family determined by RNA-seq comparing the $\log_2$ fold change from primary to metastatic tumor transcriptomes. Enriched pathways are marked on the right side of the heatmaps.

(C) Western blot analysis of Netrin-1 and actin (loading control) expression in primary tumor cell line (Ink4a.1) and four separate metastatic cell lines obtained from liver metastases.

(D) (Top) Representative immunohistochemistry images of Netrin-1 expression in human primary pancreatic tumor biopsy (i), primary patient-derived xenograft (PDX) pancreatic tumor (ii), and two metastatic pancreatic PDX tumors (iii, iv). Scale bar, 100 μm. (Bottom) Quantification of Netrin-1 expression in the TMA of PDX pancreatic tumors; n = 75 for primary, n = 18 for metastases.

(E) Expression of Netrin-1 in the Collisson et al. RNA-seq dataset of different pancreatic cancer phenotypes[13] (n = 20, quasi-mesenchymal subtype; n = 27, classical subtype; n = 19) based on expression profiling. Statistical analysis was completed using two-tailed Student's t test (*$p < 0.05$).

to the quasi-mesenchymal (QM) status of Ink4a.1, we looked to see whether high Netrin-1 expression differs among PDAC molecular subtypes. Interestingly, in the Collisson et al. dataset,[13] *NTN1* expression is significantly greater in both the QM and exocrine as compared to classical subtypes (Figure 1E).

Unc5b is the dominant Netrin-1 receptor in PDAC and functions as a dependence receptor to promote metastasis

We examined the Ink4a.1 RNA-seq dataset and found the Netrin-1 receptor that was primarily expressed in PDAC was Unc5b. We found no detectable levels of DCC and minimal to no detectable levels of Unc5a, Unc5c, and Unc5d (Figure 2A). We confirmed this by western blot in the Ink4a.1, Met25, and Met38 metastatic clones (Figure S2A). We also detected Unc5b in all cell lines of a larger panel of murine and human PDAC cells that also lacked DCC expression (Figure S2B). Using The Cancer Genome Atlas dataset in human PDAC, we also found that the dominant Netrin-1 receptor is Unc5b (Figure S2C). We then determined the impact of Netrin-1/Unc5b signaling on PDAC metastasis both *in vitro* and *in vivo*. We first confirmed the cell death mechanism of the Unc5b receptor was intact, whereby downregulation of the ligand using small interfering RNA (siRNA) in both the Ink4a.1 and Met38 cell lines led to increased apoptosis by

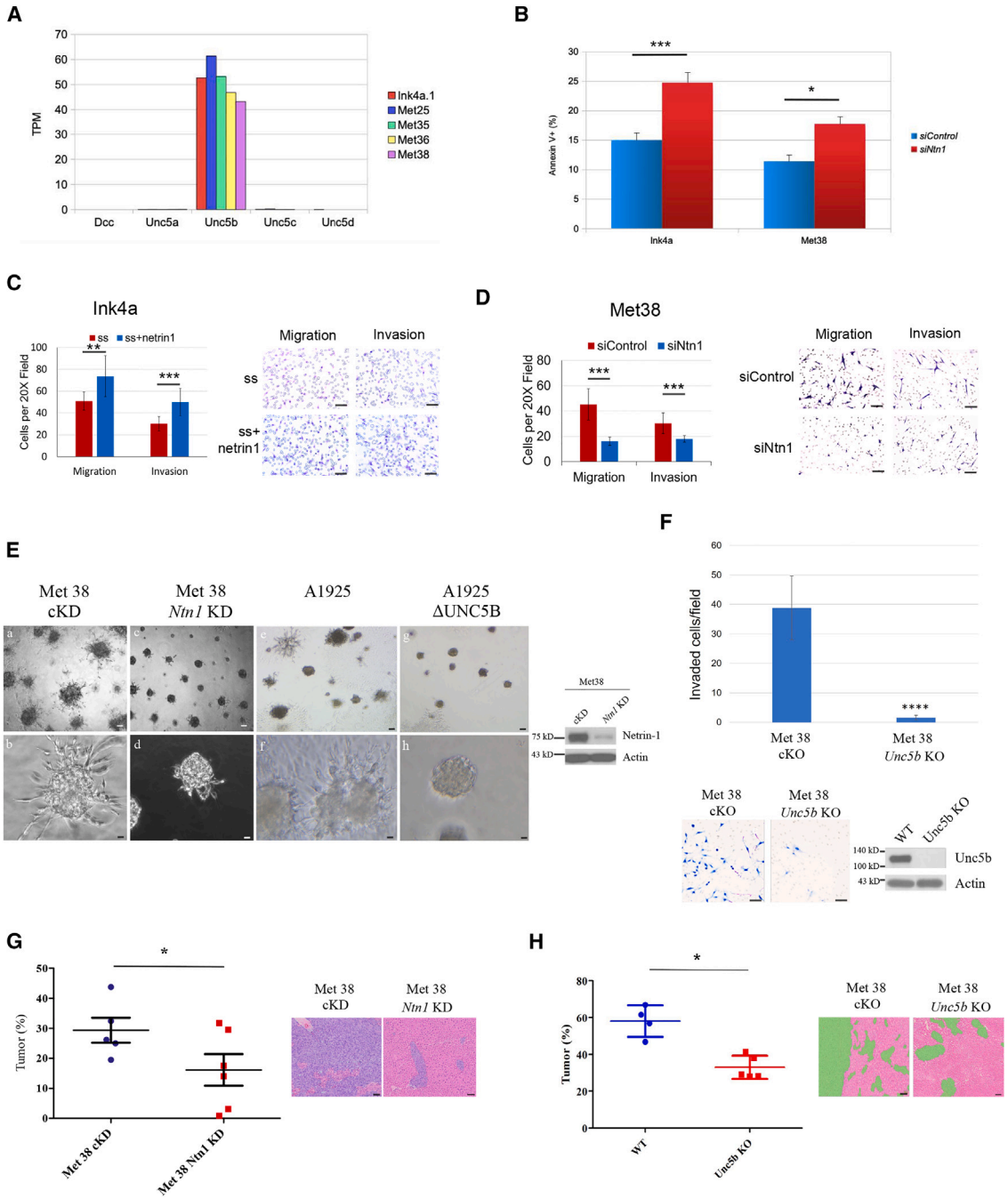

Figure 2. Unc5b is the dominant Netrin-1 receptor in PDAC and functions as dependence receptor to promote metastasis

(A) RNA-seq analysis of primary and metastatic pancreatic cancer cell-line expression of Netrin-1 receptors.

(B) Annexin V staining of primary Ink4a and metastatic Met38 cell lines transiently transfected with a non-targeting control siRNA or *Ntn1* siRNA. n = 3 in each group.

(C) (Left) Graphs of the migration and invasion analysis of serum starved Ink4a cells treated with recombinant Netrin-1. (Right) Representative images of fixed and stained cells are on the right. n = 10. Scale bars, 50 μm.

(D) (Left) Graphs of the migration and invasion analysis of Met38 cells transiently transfected with a control or *Ntn1* siRNA. (Right) Representative images of fixed and stained cells are on the right. n = 10. Scale bars, 50 μm.

(E) 3D *in vitro* sprouting assay for Met38 control KD (a, b) or *Ntn1* KD cells (c, d) and A1925 control (e, f) and Δ*Unc5b* (g, h) expressing cells. Netrin-1 knockdown was confirmed by Netrin-1 expression analysis (far right). Scale bars, 100 μm (a, c, e, g) and 20 μm (b, d, f, h).

(legend continued on next page)

annexin V staining (Figure 2B). To demonstrate that Unc5b functioned positively when ligand bound, we performed *in vitro* migration and invasion assays in the presence of recombinant Netrin-1 using the Ink4a.1 line and found that Netrin-1 significantly increased both migration and invasion (Figure 2C). Conversely, when we knocked down Netrin-1 using si*Ntn1*, we observed a significant decrease (Figure 2D). We validated *Ntn1* knockdown (KD) in these cell lines by western blot (Figure S2D). We created a stable KD of *Ntn1* in the Met38 cell line by sh*Ntn1* (KD verified by western blot, Figure S2E) whose proliferation was unchanged by *Ntn1* KD (Figure S2F). We evaluated this cell line's ability to form pseudopodia using a 3D tumor spheroid invasion assay. We found that in the control short hairpin RNA (shRNA) Met38 cells, the cells form abundant pseudopods in 7 days that were significantly attenuated in the *Ntn1* KD cells (Figure 2E). When we deleted the *Unc5b* gene from another mouse PDAC cell line, A1925, and from the Met38 cells, we also observed a significant reduction in both pseudopodia formation and cell invasion (Figures 2E and 2F, respectively). We validated these *in vitro* findings *in vivo* using a liver metastasis assay in which Met38 *Ntn1* wild type (WT) and *Ntn1* KD cells were injected into the spleen followed by splenectomy. After 10 days, mice were sacrificed and liver metastases quantitated from H&E-stained tissue sections. We found that *Ntn1* KD significantly decreased the percent tumor area of metastatic tumor growth (Figure 2G). We found a similar situation when we evaluated the *Unc5b* knockout (KO) cells by the same assay (Figure 2H). Taken together, these experiments demonstrate that Unc5b is the dominant DR in PDAC and facilitates metastasis when ligand bound and cell death when ligand unbound.

Hepatic stellate cell secretion of retinoids causes upregulation of Netrin-1 through RAR/RXR signaling

While upregulation of Netrin-1 as a survival mechanism in metastatic cancer has previously been described, the mechanism for this is unknown.[9] During liver metastasis HSCs transdifferentiate into myofibroblasts, which then secrete factors that promote tumor cell migration/invasion through a variety of mechanisms.[29] We hypothesized that HSCs might also be involved in promoting Netrin-1-mediated liver metastasis. To address this, we isolated and cultured HSCs to produce conditioned medium that was fed to the Ink4a.1 cell line over a 24-h time period. The HSC conditioned medium induced a time-dependent increase in Netrin-1 at 3, 6, and 24 h (Figure 3A). This upregulation was specific to HSCs, as we did not observe a similar increase in Netrin-1 when we incubated conditioned medium from other cell types in the liver, including hepatocytes and liver sinusoidal endothelial cells, with the Ink4a.1 cells (Figure S3A). *In vitro*, fresh isolates of HSCs cultured on plastic dishes become spontaneously activated over a period of 8 days.[30] Naive HSCs contain lipid droplets, which are specialized organelles for the storage of retinoids, and upon activation HSCs secrete these droplets extracellularly. This process can be visualized by microscopy as the intracellular droplets autofluoresce, which is lost upon activation.[31,32] We observed this process in isolated HSCs *in vitro* over a 15-day period (Figure 3B, top), confirming the loss of retinoids, and found a corresponding increase of Netrin-1 levels when Ink4a.1 cells were incubated with HSC conditioned medium from day 2 to day 15 (Figure 3B, bottom). To identify this molecule in HSC conditioned medium that upregulates Netrin-1 in tumor cells, we used size-exclusion chromatography with filter cutoff sizes of 3,000 Da (3K) and 1,000 Da (1K). Fractions were collected of the filtered and flow-through samples and analyzed for Netrin-1 upregulation by incubating them with the Ink4a.1 cells. Based upon induction of Netrin-1 by the flowthrough fractions of the 3K and 1K filters, we concluded that the molecule was less than 1,000 Da, which ruled out a macromolecule such as a protein or peptide, and hypothesized it to be a small molecule, likely a metabolite (Figure S3B). Given the major components of the HSC lipid droplets are retinoid species within this size range, we examined collected fractions of our HSC conditioned medium for evidence of retinoid species using liquid chromatography-mass spectrometry. Conditioned medium at days 8, 11, and 15 contained both retinal and retinoate (9-*cis*-retinoic acid) of molecular weight 285 and 301, respectively, while these compounds were minimally present at day 4, indicating the presence of retinoid metabolites in the conditioned medium of activated HSCs (Figure S3C). To confirm that retinoid metabolites were the molecule(s) in question, we incubated retinoic acid, 9-*cis*-retinoic acid, and retinal with the Ink4a.1 cells over 24 h and examined Netrin-1 levels and found that all three exhibited a time-dependent increase that was observed as early as 3 h (Figures 3C and S3D). The finding that retinoic acid upregulates Netrin-1 was observed in multiple murine PDAC cell lines other than the Ink4a.1 cells, suggesting this to be a common mechanism (Figure S3E).

To determine whether the upregulation of Netrin-1 in PDAC cell lines by HSC-secreted retinoic acid was mediated by retinoic acid receptors RAR/RXRs, we examined the expression levels of RAR-α, RARγ, RXRα, RXRβ, and RXRγ in three murine PDAC cell lines (Ink4a.1, K8484, and K8483). We found that all three cell lines expressed RARα and RXRα, while RARγ was expressed in the Ink4a.1 and K8383 lines but not in the K8484 line. RXRβ and RXRγ were only expressed in the K8383 line (Figure S3F). Using chromatin immunoprecipitation (ChIP), we detected the binding of RXR in the Netrin-1 promoter in response to treatment with retinoic acid (10 μM) (Figure 3D). We next performed KD experiments of both RARα and RXRα using an siRNA approach and found that KD of both led to a decrease in HSC-mediated Netrin-1 induction, and a combination of si*RAR*α/*RXR*α led to the greatest decrease in Netrin-1 induction (Figure 3E). Consistent with this result, we used a small-molecule antagonist of RXR signaling (UVI 3003) in combination with either all-*trans*-retinoic acid or 9-*cis*-retinoic acid and found that UVI 3003 suppressed the induction of these retinoids in the Ink4a.1 cells (Figure 3F). Together, these experiments indicate that activated HSCs secrete retinoic acid, which

(F) (Top) Graph of the invasion analysis of Met38 cKO (control knockout) and Met38 *Unc5b* KO cells. Representative images of fixed and stained cells are below (scale bars, 50 μm), as well as the western blot showing *Unc5b* depletion in *Unc5b* KO cells.
(G and H) H&E staining of livers after intrasplenic injection of Met38 control knockdown (KD) and Met38 *Ntn1* KD cells (G) or Met38 cKO and Met38 Unc5b KO cells (H). Quantitation of tumor area was determined by VisioPharm software. n = 6/group. Scale bars, 50 μm.
Statistical analysis was completed using two-tailed Student's t test (*$p < 0.05$, **$p < 0.01$, ***$p < 0.001$, ****$p < 0.0001$).

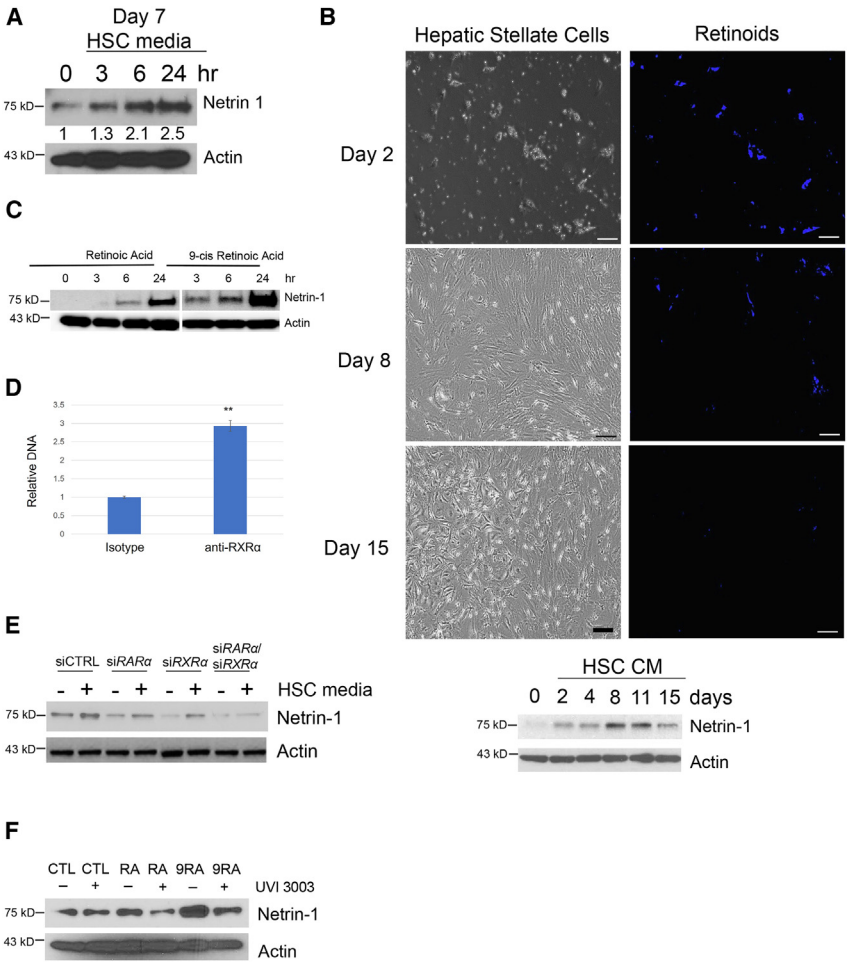

Figure 3. Hepatic stellate cell secretion of retinoids causes upregulation of Netrin-1 through RAR/RXR signaling

(A) Netrin-1 expression was analyzed by western blot following treatment with HSC conditioned medium for the indicated time points. Actin served as a loading control. The fold change of Netrin-1 expression is shown below the Netrin-1 blot.

(B) (Top) HSCs were imaged on the indicated days by brightfield or retinoid autofluorescence using the DAPI filter. Scale bars, 20 μm. (Bottom) Ink4a.1 cells were treated for 24 h with HSC conditioned medium from the top experiment. Netrin-1 expression was determined by western blot with actin as a loading control.

(C) Ink4a.1 cells were treated with retinoic acid (ATRA) and 9-*cis*-retinoic acid for the indicated times. Netrin-1 and actin expression was analyzed as before.

(D) ATRA-treated Ink4a cells were subjected to ChIP analysis of the *Ntn1* exon 1 promoter region using an isotype control or RXRα antibody, n = 4/group.

(E) Ink4a.1 cells were transfected with siRNA to RARα, RXRα, and the combination and then treated for 24 h with HSC conditioned medium. Netrin-1 and actin expression was analyzed as before.

(F) Ink4a.1 cells were treated with all-*trans*-retinoic acid (RA) or 9-*cis*-retinoic acid (9RA) ± UVI 3003 for 24 h. Netrin-1 and actin were blotted as before.

All experiments were completed in triplicate. Statistical analysis was completed using two-tailed Student's t test (**$p < 0.01$).

in turn upregulates Netrin-1 through RAR/RXR signaling. RXR signaling appears to be more important, as 9-*cis*-retinoic acid has the biggest effect on Netrin-1 induction (Figure 3C) and targets RXR preferentially over RAR.

Elf3 increases expression of Netrin-1 in human and mouse pancreatic cancer cells

We noted that a number of cell lines derived from liver metastases from Ink4a.1 primary tumors retained upregulated expression of Netrin-1 despite no longer being in the presence of HSCs or retinoic acid (Figure 1C), suggesting that these cells underwent epigenetic reprogramming, possibly in response to retinoic acid, as this has been shown to modulate chromatin.[33] We examined our ATAC-seq data (Figure S1B) at the *Ntn1* locus for evidence of differential peaks between the metastatic and parental cells and did not find a difference (Figure S3G); however, we did find the locus of transcription factor Elf3 to be more open in the Met38 cell line (Figure 4A). *Elf3* mRNA expression was also upregulated in the Met38 cell line as well as in all other cell lines (Met25, Met35, Met36, and Met72) derived from metastatic Ink4a.1 tumors (Figure S3H).

Like *Ntn1*, transcription of *Elf3* was strongly induced by retinoic acid in pancreatic cancer cell lines with doses as low as 5 nM (Figures 4B and S3I). Binding of RAR to the Elf3 promoter was also detected by ChIP (Figure 4C). Since ELF3 has been shown to cause EMT in hepatocellular cancer cells,[34] we tested whether retinoic acid can also promote EMT in pancreatic cancer cells using a set of cell lines derived from an alternative PDAC model (Ptf1a-Cre;LSL-Kras^{G12D};Arid1a$^{f/f}$ [KPCA]).[35] As shown in Figure 4D, the epithelial marker protein E-cadherin was decreased by retinoic acid treatment, while the mesenchymal marker protein vimentin increased in a dose-dependent manner. We hypothesized that Elf3 may upregulate Netrin-1 directly, as there are several Elf3 consensus binding sites in the *Ntn1* promoter conserved across species. Using ChIP, we confirmed that Elf3 bound the *Ntn1* promoter (Figure 4E). We observed an induction of *Ntn1* when Elf3 was overexpressed in the Ink4a.1 cells (Figure 4F). Alternatively, when CRISPR-Cas9 was used to reduce expression of *Elf3* in the Met38 cell line, there was decreased induction of *Ntn1* by retinoic acid (Figure 4G). In a human PDAC cell line, Miapaca-2, siRNA-dependent KD of *ELF3* expression (Figure S3J, right) caused a sharp decrease in *NTN1* expression (Figure S3J, left). Of note, we did not concomitantly silence expression of the retinoic acid receptors in these experiments. These results demonstrate that *Elf3* regulates *Ntn1*, and this can occur directly by retinoic acid signaling (through RAR/RXR) or indirectly by epigenetic reprogramming.

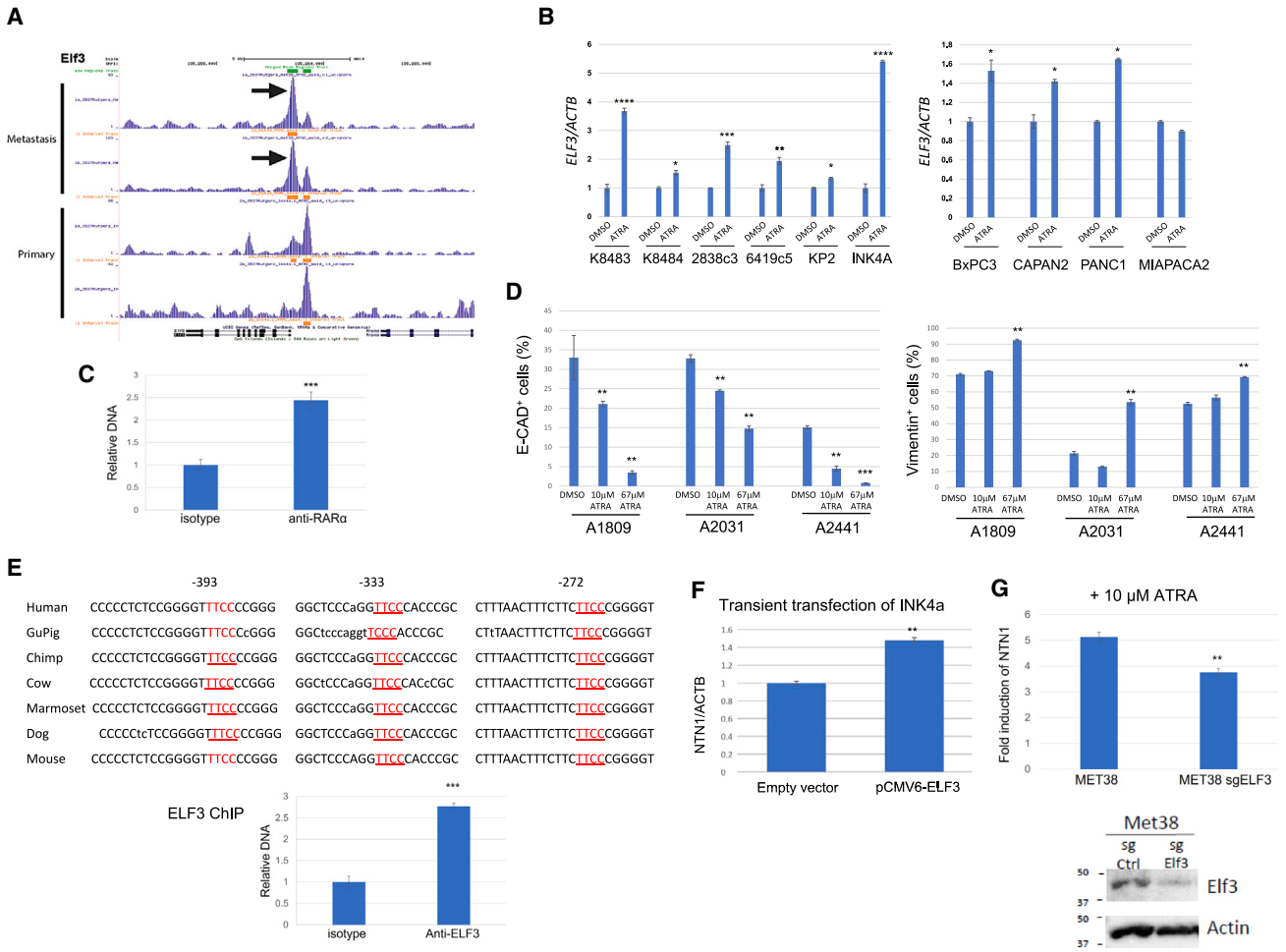

Figure 4. Elf3 increases expression of Netrin-1 in human and mouse pancreatic cancer cells

(A) ATAC-seq analysis of the Elf3 promoter for metastatic Met38 and primary Ink4a.1 pancreatic cancer cells, n = 2/group.

(B) Expression of Elf3 was determined by qPCR in multiple primary and metastatic mouse (left) and human (right) pancreatic cancer cell lines treated with 10 μM all-*trans*-retinoic acid (ATRA) for 18 h. Actin expression was used for normalization. In all cases except for MIAPACA-2, the increase in Elf3 mRNA was statistically significant by two-tailed t test, n = 3/group.

(C) ChIP experiment to demonstrate that RARα interacts with the Elf3 promoter, n = 4/group.

(D) Following 7 days of treatment with DMSO or varying concentrations of ATRA, the percentages of E-cadherin-positive (left) and vimentin-positive (right) cells were determined by flow cytometry in three cell lines, each of which had been developed from pancreatic tumors generated by different KPC-*Arid1a*$^{-/-}$ mice, n = 3/group.

(E) The top panel shows conservation of consensus Elf3 transcription factor binding sequence within the Netrin-1 promoter in a variety of species, while the bottom panel shows results of a ChIP experiment indicating that Elf3 interacts with this region on the mouse *Ntn1* gene. (F) Ink4a.1 cells were transfected for 72 h with pCMV6 or with pCMV6-Elf3, followed by qPCR to assay Netrin-1 transcription. Actin was used as a normalization control, n = 3/group.

(G) Met38 sgControl and sgElf3 were treated with DMSO or 10 μM ATRA for 18 h and analyzed for Netrin-1 RNA expression. The top graph shows the fold change of Netrin-1 expression for ATRA vs. DMSO, n = 3. All experiments were completed at least in duplicate and represent mean ± SEM. In the bottom panel the reduction of Elf3 protein is demonstrated by western blot analysis; positions of molecular weight markers, in kDa, are indicated.

Statistical analysis was completed using two-tailed Student's t test (*p < 0.05, **p < 0.01, ***p < 0.001, ****p < 0.0001).

Netrin-1 on the surface of extracellular vesicles promotes hepatic metastasis by activating HSCs

Netrin-1 and its receptors have been shown to be expressed on a variety of cell types including cancer-associated fibroblasts (CAFs)[36]; thus, we hypothesized that tumor-cell-secreted Netrin-1 might be involved in HSC activation. We incubated recombinant Netrin-1 with freshly isolated HSCs and observed a time-dependent increase in the expression of genes associated with the activated HSC phenotype (*Acta2*, *Col1a1*, and *Lox*) (Figure 5A). To find out whether this effect could be observed *in vivo*, we created an *Ntn1* KO in the Ink4a.1 cell line. We confirmed a lack of *Ntn1* expression in two different KO clones (P2A4, P5E11) by qPCR analysis (Figure S4A). We implanted the Ink4a.1 *Ntn1* WT and KO cells orthotopically and allowed primary pancreatic tumors to develop. After 20 days the mice were sacrificed and their livers harvested to assess for *in vivo* HSC activation. Of note, there was no significant difference in size of the *Ntn1* KO primary tumors compared to the *Ntn1* WT (Figure S4B)

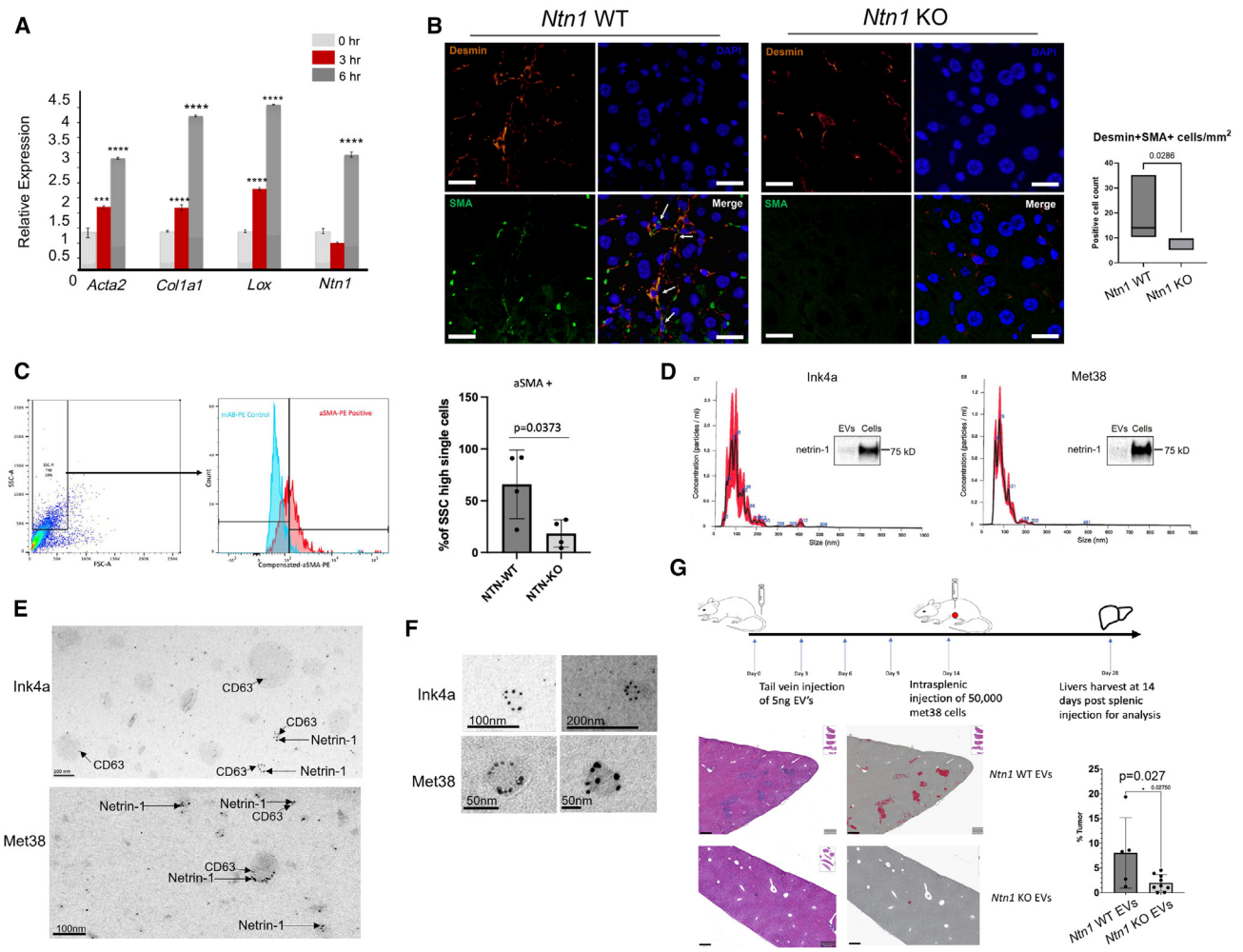

Figure 5. Netrin-1 on the surface of extracellular vesicles promotes hepatic metastasis by activating HSCs

(A) Expression of HSC activation markers was determined by qPCR following treatment of HSCs with recombinant Netrin-1 at the indicated time points, n = 6/group.

(B) *In vivo* activation of HSCs was determined by Desmin and SMA immunofluorescence staining of livers from mice orthotopically injected with Ink4a.1 WT and *Ntn1* KO cells (left). Quantitation of Desmin$^+$/SMA$^+$ HSC cells (right) was determined (n = 10). Scale bars, 50 μm.

(C) Activated HSCs were identified and quantitated by flow cytometry using high side scatter and SMA staining, n = 4.

(D) NanoSight software analysis on EVs from Ink4a and Met38 cells showing the size of the analyzed EVs. Inset: Netrin-1 expression analysis of cellular and EV fraction by western blot.

(E) TEM analysis on EVs harvested from Ink4a.1 and Met38 cells using Netrin-1 antibody coupled to 15-nm gold beads. Representative images showing the frequency of EVs labeled with Netrin-1 and specific EV marker, CD63. Scale bar, 100 nm.

(F) Enlargement of representative Netrin-1-positive EVs. Scale bars, 100 nm (Ink4a, left), 200 nm (Ink4a, right), and 50 nm (Met38).

(G) (Top) Schema for the *in vivo* experimental metastasis model used to demonstrate EV priming of the liver for pancreatic cancer metastatic seeding. (Bottom left) H&E staining of livers obtained from mice primed with Netrin-1-containing or Netrin-1 null EVs prior to pancreatic cancer cell seeding. (Bottom right) Percentage of tumor area compared to total liver lobe area shows significant decrease of priming the microenvironment with *Ntn1* KO EVs compared to WT EVs. n = 10. Scale bars, 200 μm.

All experiments were completed at least in duplicate. Statistical analysis was completed using two-tailed Student's t test (***p < 0.001, ****p < 0.0001).

and, in addition, the livers of these mice did not show evidence of macro- or microscopic metastases (data not shown). Since the Ink4a.1 cells express the Cre recombinase and the FVB host mice that are used to create pancreatic tumors do not, we developed a qPCR-based assay for Cre recombinase DNA in liver tissue as a sensitive means of detecting metastatic cells in the liver, particularly when it is difficult to detect them by immunofluorescent techniques. We found that at 20 days post injection the amount of Cre recombinase in the liver of mice injected with either *Ntn1* WT or KO cells was not significantly different, and in fact there was a trend toward an increase in the *Ntn1* KO group (Figure S4C). This indicates that at this early stage of primary tumor development, there was evidence of distant metastasis that was not significantly different in either the *Ntn1* WT or KO tumors.

To determine whether there was a difference in HSC activation *in vivo*, we performed dual immunofluorescence on the livers of

mice harboring either *Ntn1* WT or KO pancreatic tumors using the HSC marker desmin. We used smooth muscle actin (SMA) to indicate transdifferentiation to the myofibroblast state. We quantified double-positive desmin/SMA cells and found a significant increase in the mice with *Ntn1* WT compared to KO tumors (Figure 5B). As an alternative approach to evaluating the activation state of HSCs in the liver, we used flow cytometry to identify HSCs by high side scatter (SSC).[37] We repeated the orthotopic pancreatic tumor experiment with either *Ntn1* WT vs. KO cells, and at 20 days post injection harvested livers for cell isolation and stained the cells with an antibody to SMA. We gated the top 10% of high-SSC events for HSC isolation as previously described and then quantified the SMA^+ population. This population of HSCs represents the early activated state before the HSCs have fully released their vitamin A stores. We found a significantly greater number of high-SSC/SMA^+ cells in the livers of mice harboring the Ntn1 WT vs. KO tumors (Figure 5C). This indicates that Ntn1 activates HSCs both *in vitro* and *in vivo*, and also suggests that this intercellular communication could be through not only a short-range but also a long-range mechanism.

Although Netrin-1 is a secreted protein, its laminin structure causes it to tightly associate with extracellular matrix proteins rather than enter the blood. Interestingly, we did detect the presence of Netrin-1 in tumor-derived EVs, which have been shown to enter the bloodstream and to play a role in pre-metastatic niche formation in pancreatic and other cancers.[38,39] We isolated EVs from conditioned medium of Netrin-1-expressing cells (Ink4a.1, Met38) using modified ultracentrifugation protocols suitable for EV isolation from conditioned medium.[40,41] We determined the size distribution of the different pellets and concentration using NanoSight software (nanoparticle tracking analysis [NTA]). All EV populations presented a peak in particle size around 100 nm (Figure 5D). Western blot analysis was used to assess Netrin-1 presence in EVs in each of these cell lines (Figure 5D). To investigate Netrin-1's localization, transmission electron microscopy (TEM) analysis was performed using a commercial anti-Netrin-1 antibody coupled with 15-nm gold beads to analyze EVs derived from Ink4a and Met38 cell lines. In parallel, a commercial CD63 tetraspanin antibody was coupled with 5-nm gold beads as a positive control of EV labeling. We performed this analysis without permeabilization such that detection of a positive signal indicated that Netrin-1 is located at the vesicle surface. TEM detected Netrin-1 localization at the surface of EVs of InK4a and Met38 cells, respectively, with a frequency of 10% and 50% of all EVs (Figures 5E and 5F). As Netrin-1 is upregulated in the Met38 cell line as compared to Ink4a.1, we detected a significantly higher number of Netrin-1^+ EVs among the $CD63^+$ EVs (Figure S4D). As an alternative approach, we harvested EVs from conditioned medium by immunoaffinity isolation in both Ink4a.1 and Met38 cells and verified the presence of EVs with expression of alix, a known EV marker. Netrin-1 was detected in the EV fraction, with the Met38 cells showing a greater yield of Netrin-1 (Figure S4E). We also prepared EVs from Ink4a.1 *Ntn1* WT and KO cells and demonstrated Netrin-1 detection in the conditioned medium as well as the EV fraction from *Ntn1* WT cells, while *Ntn1* KO EVs were devoid of Netrin-1 expression (Figure S4F). We further confirmed that this fraction contained EVs by TEM, revealing that both the preparation from *Ntn1* WT and *Ntn1* KO cells exhibited similarly sized particles (Figure S4G). To determine the generality of Netrin-1 presence in EVs, we isolated EVs from three human lung cancer cell lines (A549, H322, and H358) that were of size (100 nm) by NTA similar to that of EVs from the Ink4a.1 and Met38 lines (Figure S5A). Netrin-1 was present in EVs of H322 and H358 but not in A549 (Figure S5B, with CD9 and Flottilin-1 as EV markers). TEM analysis of the H358 and A549 cells for CD63 demonstrated the presence of CD63 on the surface of all EVs, while Netrin-1 was only present in the H358 EVs (Figure S5C). This suggests a general mechanism of Netrin-1 localization in EVs of cancer cells.

We then employed the splenic liver metastasis assay to determine whether Netrin-1^+ EVs functionally contributed to the metastatic process. To this end, we harvested EVs from Ink4a.1 *Ntn1* WT and *Ntn1* KO cells by immunoaffinity isolation. For this *in vivo* experiment, mice were pre-treated with EVs prepared from Ink4a.1 *Ntn1* WT and *Ntn1*KO cells for 2 weeks prior to injecting the Met38 cells intrasplenically. The dose and schedule of EVs was previously shown to facilitate liver metastatic niche formation in pancreatic cancer.[38] After 14 days, the mice were sacrificed and livers harvested to assay for differences in metastatic burden. We found that the mice injected with the *Ntn1* KO EVs exhibited a marked decrease in the metastatic burden as evidenced by gross examination of the liver and histologic quantitation (Figure 5G). These data indicate that Netrin-1 is present at the surface of EVs from tumor cells and that these EVs are functionally relevant to liver metastasis through HSC activation.

Netrin-1 interference suppresses metastasis and increases survival in murine PDAC models

While the Unc5b receptor facilitates metastasis, due to its function as a DR it also provides a pathway to therapeutically target these metastatic tumor cells by interfering with Netrin-1 signaling to initiate apoptosis. We evaluated the potential of Netrin-1 as a therapeutic target in PDAC by first using the *in vivo* Ink4a.1 liver metastasis assay to assess quantitation of metastatic burden and overall survival as endpoints. One day before splenic injection of the Ink4a.1 tumor cells, mice were treated with a monoclonal antibody to Netrin-1 (mAbNtn1) every other day for 14 days before the mice were sacrificed and the metastatic burden of the livers quantified. We found that Netrin-1 interference significantly decreased the number of metastatic colonies as compared to the vehicle control (Figure 6A). Likewise, when we evaluated the same model for overall survival, we found that Netrin-1 interference significantly improved overall survival. All of the PBS-treated mice succumbed to their PDACs by day 46 while three out of nine mice in the mAbNtn1 group remained alive beyond 200 days. The median survival was 37 days for the control and 56 days for the mAb-Ntn1 group ($p \leq 0.008$) (Figure 6B). To confirm these results, we turned to another liver metastatic model using a cell line (KPC3) derived from the Pdx1-Cre;LSL-$Kras^{G12D}$;$Trp53^{f/f}$ model injected directly into the portal vein of C57Bl/6J mice and treated with either immunoglobulin G (IgG) control or mAbNtn1 twice per week for 3 weeks prior to sacrifice. We quantified sections of liver stained for CK17 as a marker for tumor cells and found that anti-Netrin-1 therapy significantly reduced the metastatic burden (Figure 6C). The Netrin-1 levels in the KPC3 cell line were not detectable by western blot (Figure 6D), but when the cells engrafted in

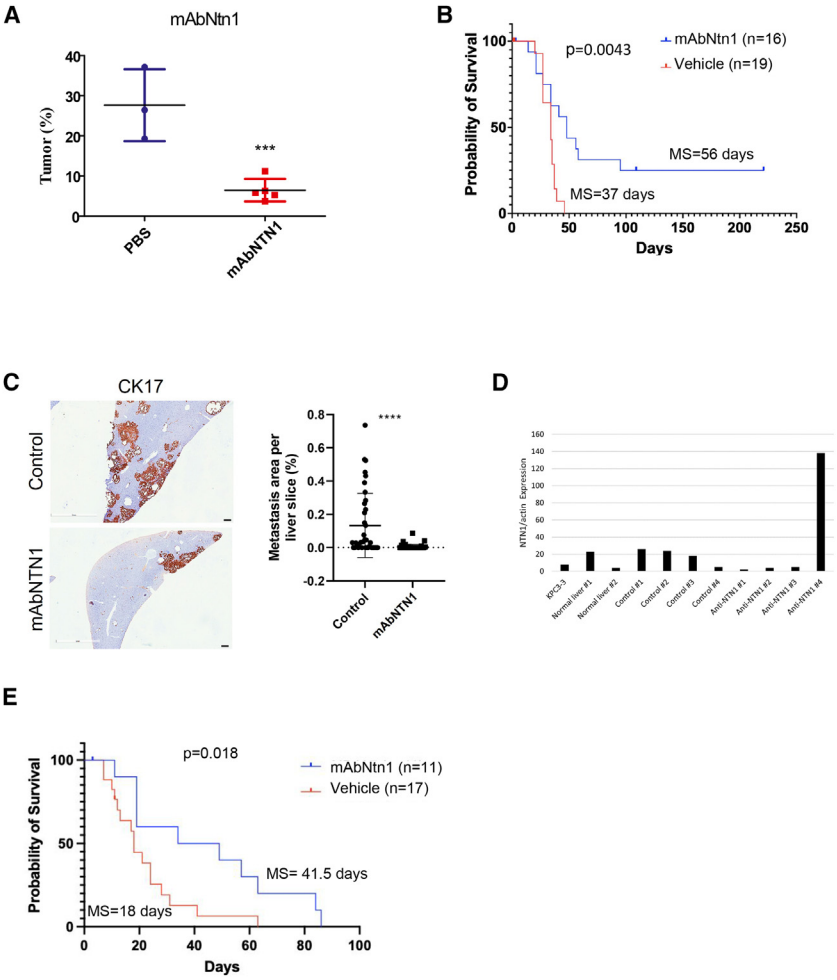

Figure 6. Netrin-1 interference suppresses metastasis and increases survival in murine PDAC models

(A) Mice were pretreated with mAbNtn1 for 2 days and intrasplenically injected with 50,000 Ink4a.1 cells. Antibody treatment (10 mg/kg) continued every 2 days until liver harvest at day 14. Percentage tumor area in the liver was quantified as before (n = 5).

(B) Kaplan-Meier graph showing survival of mice injected intrasplenically with 20,000 Ink4a.1 cells using mAbNtn1 (n = 16) as adjuvant treatment or vehicle (n = 19). Note that three mAbNtn1-treated mice have not recurred beyond day 200.

(C) Immunohistochemistry of CK17-stained livers from C57Bl/6J mice injected via portal vein injection with KPC3 cells (left) and treated with IgG control or mAbNtn1, n = 10/group. Percentage of tumor metastasis area was quantified as before, n = 5 sections/mouse. Note the significant reduction in mice treated with anti-Netrin-1 antibody (right). Scale bars, 200 μm.

(D) Normalized Netrin-1 expression in KPC3 cells, normal liver, hepatic KPC3 metastases from control IgG-treated mice, and hepatic KPC3 metastases from mAbNtn1-treated mice as quantified by western blot.

(E) Kaplan-Meier plot showing survival of KPC mice treated with IgG vehicle and mAbNtn1 antibodies. The vehicle group (n = 17) had MS = 18 days, while the mAbNtn1 group (n = 11) had MS ∼ 42 days, a doubling of lifespan.

All experiments were completed at least in duplicate. Statistical analysis was completed using two-tailed Student's t test (***p < 0.001, ****p < 0.0001).

the liver and formed tumors in both the IgG control and mAbNtn1-treated mice, Netrin-1 levels significantly increased, consistent with our observations of the Ink4a.1 model (Figure 1C). There was a marked decrease in Netrin-1 levels in the livers of mAbNtn1-treated mice compared to the IgG controls (Figure 6D). To evaluate the efficacy of anti-Netrin-1 on survival in an autochthonous mouse model, we used the Pdx-1;Kras$^{G12D/+}$;p53$^{R172H/+}$ (KPC) model in which mice were monitored for primary tumor growth and randomized to either vehicle control vs. mAbNtn1 when a dominant tumor was detected by ultrasound at 4–5 mm. We found that the mAbNtn1 significantly improved the median survival, from 18 days in the control to 42 days in mAbNtn1 (p = 0.018) (Figure 6E). Taken together, these data suggest that anti-Netrin-1 decreases metastasis and improves survival in pre-clinical pancreatic cancer models.

DISCUSSION

The biology of metastatic PDAC remains poorly understood, but evidence now exists that it is largely driven by epigenetic mechanisms that govern cell plasticity.[1] The source of these mechanisms and their timing during tumor progression remains unclear. Here we demonstrate that one source of this plasticity is driven by the microenvironment of the metastatic niche, as evidenced by the upregulation of the axon guidance molecule, Netrin-1, signaling through its receptor Unc5b to promote dissemination and metastatic tumor cell survival. Most importantly, because of the unique cell death mechanism of DRs triggered upon interference with ligand binding, this upregulation also confers therapeutic vulnerability to metastatic PDAC.

While Netrin-1 has been shown to be upregulated in metastases of other solid organ cancers such as breast and colon,[9,42] the mechanism of this is unknown. As such, the feedforward mechanism we have found through Netrin-1 activating HSCs to then secrete retinoic acid, which then upregulates Netrin-1 in metastatic tumor cells, represents a significant advancement in Netrin-1 tumor biology and emphasizes the role of the metastatic niche in driving this aspect of PDAC biology (Figure 7). Our data suggest that inhibition of RXR or dual RXR/RAR signaling could potentially be useful for hepatic metastases either alone or in combination with anti-Netrin-1 therapy. There are currently no inhibitors of RXR or RAR signaling available in the clinic, and the inhibitors that exist for research purposes (such as the one used here) are not optimized for *in vivo* use. Another strategy would be to combine Netrin-1 inhibitors with inhibitors of HSC activation, which are currently being investigated to treat liver fibrosis.[43] Interestingly, dietary intake of retinol or oleic acid

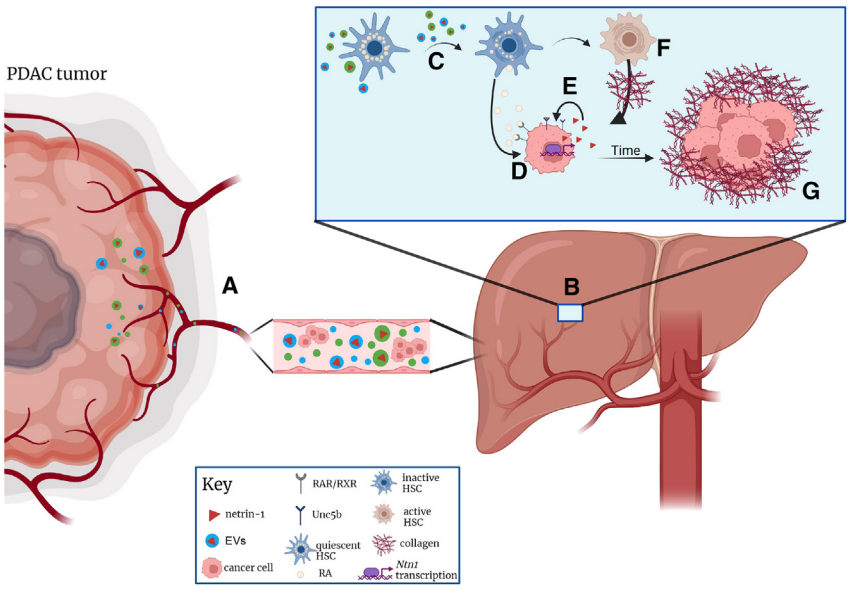

Figure 7. The Netrin-1 feedforward mechanism that promotes liver metastasis

EVs containing Netrin-1 activate HSCs through both long-range (A) and possibly short-range communication upon dissemination in the liver (B). Upon activation by Netrin-1, HSCs dump their retinoic acid stores (C). The free retinoic acid is taken up by DTCs by their retinoic acid receptors (D), leading to upregulation of Netrin-1 directly and indirectly through Elf3 upregulation. Through autocrine signaling (E) by Unc5b receptors, newly arrived DTCs increase survival potential through Netrin-1 excretion. In addition, activated hepatic stellate cells deposit collagen into the microenvironment (F), which over time allows macrometastases to become established in the liver (G).

has been shown to inhibit liver fibrosis by inhibiting HSC[44,45] but has not been investigated as a strategy to inhibit liver metastasis.

The finding of Netrin-1 on the surface of EVs represents a significant contribution to the Netrin-1 field, as it shows that Netrin-1 can function in both long- and short-range intercellular communication. This fits well with previous reports showing that secreted Netrin-1 (not associated with EVs) binds to the surface of cells through heparin sulfate functioning in an autocrine manner to guide axons, making it difficult to perform this type of intercellular communication.[5,46] While it has been shown that exosomes from pancreatic cancer can facilitate liver metastasis by preparing the metastatic niche, the mechanism was shown to be distinct from ours in that the exosomes were taken up by Kupffer cells, which led to the secretion of cytokines that acted locally within the liver to activate HSCs.[38] Both investigations suggest the importance of HSC activation to contribute toward making a more hospitable environment for the survival of metastatic PDAC cells.

The vast majority of PDAC patients harbor disseminated disease; thus, a therapy that targets the biology of metastatic PDAC (such as Netrin-1 signaling) could have a significant clinical impact. NP137 is the first-in-class humanized monoclonal antibody specific to Netrin-1 which targets the V2 subdomain that is critical for binding to the Unc5 receptors.[47] NP137 was shown to be safe in a phase I clinical trial for multiple solid organ cancers (NCT02977195) and is now being evaluated in phase II in patients with advanced gynecological cancers in a follow-up study of locally advanced PDAC patients in combination with FOLFIRINOX (NCT05546853).[48]

Limitations of the study

There are several limitations of this study. Given that the primary source of retinoic acid is the liver, this raises the question as to the existing mechanism in other organs. Given that the microenvironment of other organs is vastly different, it is likely that other drivers of cell plasticity are likely driving Netrin-1 upregulation. The discovery that Netrin-1-positive EVs activate HSCs and contribute to liver metastasis through HSC activation indicates that EV-associated Netrin-1 is functionally relevant to liver metastasis. While we provide evidence that this can occur through a long-range mechanism, it is possible that this occurs through both long- and short-range mechanisms. Our data provide preclinical evidence to support a trial of NP137 in metastatic PDAC patients. Virtually all PDAC patients (both early and late stages) harbor disseminated disease and, as such, the data do not inform whether NP137 will have equal efficacy on already established metastases vs. micrometastatic disease. The pre-clinical data would support the latter, which is why we speculate that the clinical setting that would most benefit from Netrin-1 therapy would be in patients undergoing surgical resection, where anti-Netrin-1 therapy can prevent the progression of micrometastatic disease to clinically detectable disease.

Metastatic relapse occurs in the majority (>80%) of patients following curative-intent surgery due to a large burden of disseminated tumor cells present at the time of surgery. Our data suggest that anti-Netrin-1 therapy could potentially have a significant impact in this circumstance. We have now entered the era where the molecular subtype in PDAC has been shown to correlate with differences in survival in response to chemotherapy, with basal or QM tumors being associated with chemotherapy resistance and a worse survival. Therapies for QM tumors are needed, and the finding that Netrin-1 is upregulated in QM tumors supports the investigation of NP137 in PDAC for differential responses in classical vs. basal/QM tumors.

STAR★METHODS

Detailed methods are provided in the online version of this paper and include the following:

- KEY RESOURCES TABLE
  - Lead contact

SUPPLEMENTAL INFORMATION

Supplemental information can be found online at https://doi.org/10.1016/j.celrep.2023.113369.

ACKNOWLEDGMENTS

This work was partially funded by a grant from the Pancreatic Cancer Action Network to D.R.C. and P.M. as well as funds provided by the Wilmot Cancer Institute to D.R.C. Funding from the following were also provided to P.M.: Ligue Contre Le Cancer, INCA, ANR, and Institut Convergence PLAsCAN. I.A. acknowledges funding from NCI (CA-06927, R01CA188430, K22CA160725, R21CA164205, R21CA231252). S.F. received a fellowship from Ligue Contre Le Cancer. Funding support from the Pancreatic Cancer Action Network was also provided to C.O. by the Francoise Wallace Monahan Fund. We thank Alain Brisson for advice on exosome isolation and identification. We thank Guy Montelione for assistance with size-exclusion chromatography. We would like to acknowledge Tracy Withers and Aizhan Surumbayeva for their assistance with animal studies, and Zachary Sechrist and Asra Asad for their assistance with *in vitro* migration studies. We would like to acknowledge the URMC Wilmot Cancer Institute flow cytometry shared resource. Services, results, and/or products in support of the research were generated by Rutgers Cancer Institute of New Jersey Flow Cytometry & Cell Sorting Shared Resource P30CA072720-5921 and Metabolomics Shared Resource supported, in part, with funding from NCI-CCSG P30CA072720-5923. We acknowledge the contribution of the SFR Santé Lyon-Est (UAR3453 CNRS, US7 Inserm, UCBL) facility: CIQLE (a LyMIC member), especially Elisabeth Errazuriz-Cerda, for their help on the TEM imaging.

AUTHOR CONTRIBUTIONS

C.D.: investigation, formal analysis, validation, data curation, writing – original draft, writing – review & editing. A.C.: investigation, formal analysis, validation, data curation. C.H.: investigation, formal analysis, validation, data curation, writing – original draft, writing – review and editing. C.O.: investigation, formal analysis. M.B.: investigation. S.F.: investigation. A.B.: investigation, formal analysis, writing – original draft. B.D.: investigation. D.G.: investigation. X.S.: investigation, formal analysis. J.P.: formal analysis. A.H.: resources. S.D.: formal analysis. W.N.: investigation, resources. F.S.: investigation. C.S.: investigation. D.B.V.-C: investigation. O.P.: investigation. L.W.: investigation, validation. I.A.: methodology, supervision. P.M.: supervision, writing – original draft, funding acquisition. D.R.C.: conceptualization, methodology, validation, writing – original draft, writing – review and editing, visualization, supervision, project administration, funding acquisition.

DECLARATION OF INTERESTS

The authors declare no competing interests.

Received: January 3, 2023
Revised: September 4, 2023
Accepted: October 18, 2023
Published: November 3, 2023

REFERENCES

1. McDonald, O.G., Li, X., Saunders, T., Tryggvadottir, R., Mentch, S.J., Warmoes, M.O., Word, A.E., Carrer, A., Salz, T.H., Natsume, S., et al. (2017). Epigenomic reprogramming during pancreatic cancer progression links anabolic glucose metabolism to distant metastasis. Nat. Genet. *49*, 367–376. https://doi.org/10.1038/ng.3753.
2. Pitarresi, J.R., Norgard, R.J., Chiarella, A.M., Suzuki, K., Bakir, B., Sahu, V., Li, J., Zhao, J., Marchand, B., Wengyn, M.D., et al. (2021). PTHrP Drives Pancreatic Cancer Growth and Metastasis and Reveals a New Therapeutic Vulnerability. Cancer Discov. *11*, 1774–1791. https://doi.org/10.1158/2159-8290.CD-20-1098.
3. Biankin, A.V., Waddell, N., Kassahn, K.S., Gingras, M.C., Muthuswamy, L.B., Johns, A.L., Miller, D.K., Wilson, P.J., Patch, A.M., Wu, J., et al. (2012). Pancreatic cancer genomes reveal aberrations in axon guidance pathway genes. Nature *491*, 399–405. https://doi.org/10.1038/nature11547.
4. Mehlen, P., Delloye-Bourgeois, C., and Chédotal, A. (2011). Novel roles for Slits and netrins: axon guidance cues as anticancer targets? Nat. Rev. Cancer *11*, 188–197. https://doi.org/10.1038/nrc3005.
5. Serafini, T., Kennedy, T.E., Galko, M.J., Mirzayan, C., Jessell, T.M., and Tessier-Lavigne, M. (1994). The netrins define a family of axon outgrowth-promoting proteins homologous to C. elegans UNC-6. Cell *78*, 409–424. https://doi.org/10.1016/0092-8674(94)90420-0.
6. Lai Wing Sun, K., Correia, J.P., and Kennedy, T.E. (2011). Netrins: versatile extracellular cues with diverse functions. Development *138*, 2153–2169. https://doi.org/10.1242/dev.044529.
7. Gibert, B., and Mehlen, P. (2015). Dependence Receptors and Cancer: Addiction to Trophic Ligands. Cancer Res. *75*, 5171–5175. https://doi.org/10.1158/0008-5472.CAN-14-3652.
8. Delloye-Bourgeois, C., Brambilla, E., Coissieux, M.M., Guenebeaud, C., Pedeux, R., Firlej, V., Cabon, F., Brambilla, C., Mehlen, P., and Bernet, A. (2009). Interference with netrin-1 and tumor cell death in non-small cell lung cancer. J. Natl. Cancer Inst. *101*, 237–247. https://doi.org/10.1093/jnci/djn491.
9. Fitamant, J., Guenebeaud, C., Coissieux, M.M., Guix, C., Treilleux, I., Scoazec, J.Y., Bachelot, T., Bernet, A., and Mehlen, P. (2008). Netrin-1 expression confers a selective advantage for tumor cell survival in metastatic breast cancer. Proc. Natl. Acad. Sci. USA *105*, 4850–4855. https://doi.org/10.1073/pnas.0709810105.

10. Dumartin, L., Quemener, C., Laklai, H., Herbert, J., Bicknell, R., Bousquet, C., Pyronnet, S., Castronovo, V., Schilling, M.K., Bikfalvi, A., and Hagedorn, M. (2010). Netrin-1 mediates early events in pancreatic adenocarcinoma progression, acting on tumor and endothelial cells. Gastroenterology *138*, 1595–1606, 1606.e1-8. https://doi.org/10.1053/j.gastro.2009.12.061.

11. Collisson, E.A., Trejo, C.L., Silva, J.M., Gu, S., Korkola, J.E., Heiser, L.M., Charles, R.P., Rabinovich, B.A., Hann, B., Dankort, D., et al. (2012). A central role for RAF–>MEK–>ERK signaling in the genesis of pancreatic ductal adenocarcinoma. Cancer Discov. *2*, 685–693. https://doi.org/10.1158/2159-8290.CD-11-0347.

12. Bardeesy, N., Aguirre, A.J., Chu, G.C., Cheng, K.H., Lopez, L.V., Hezel, A.F., Feng, B., Brennan, C., Weissleder, R., Mahmood, U., et al. (2006). Both p16(Ink4a) and the p19(Arf)-p53 pathway constrain progression of pancreatic adenocarcinoma in the mouse. Proc. Natl. Acad. Sci. USA *103*, 5947–5952. https://doi.org/10.1073/pnas.0601273103.

13. Collisson, E.A., Sadanandam, A., Olson, P., Gibb, W.J., Truitt, M., Gu, S., Cooc, J., Weinkle, J., Kim, G.E., Jakkula, L., et al. (2011). Subtypes of pancreatic ductal adenocarcinoma and their differing responses to therapy. Nat. Med. *17*, 500–503. https://doi.org/10.1038/nm.2344.

14. Erstad, D.J., Sojoodi, M., Taylor, M.S., Ghoshal, S., Razavi, A.A., Graham-O'Regan, K.A., Bardeesy, N., Ferrone, C.R., Lanuti, M., Caravan, P., et al. (2018). Orthotopic and heterotopic murine models of pancreatic cancer and their different responses to FOLFIRINOX chemotherapy. Dis. Model. Mech. *11*, dmm034793. https://doi.org/10.1242/dmm.034793.

15. Erstad, D.J., Sojoodi, M., Taylor, M.S., Jordan, V.C., Farrar, C.T., Axtell, A.L., Rotile, N.J., Jones, C., Graham-O'Regan, K.A., Ferreira, D.S., et al. (2020). Fibrotic Response to Neoadjuvant Therapy Predicts Survival in Pancreatic Cancer and Is Measurable with Collagen-Targeted Molecular MRI. Clin. Cancer Res. *26*, 5007–5018. https://doi.org/10.1158/1078-0432.CCR-18-1359.

16. Takahashi, K., Ehata, S., Koinuma, D., Morishita, Y., Soda, M., Mano, H., and Miyazono, K. (2018). Pancreatic tumor microenvironment confers highly malignant properties on pancreatic cancer cells. Oncogene *37*, 2757–2772. https://doi.org/10.1038/s41388-018-0144-0.

17. Thiery, J.P., Acloque, H., Huang, R.Y.J., and Nieto, M.A. (2009). Epithelial-mesenchymal transitions in development and disease. Cell *139*, 871–890. https://doi.org/10.1016/j.cell.2009.11.007.

18. Tsai, J.H., and Yang, J. (2013). Epithelial-mesenchymal plasticity in carcinoma metastasis. Genes Dev. *27*, 2192–2206. https://doi.org/10.1101/gad.225334.113.

19. Wu, M., Li, X., Liu, R., Yuan, H., Liu, W., and Liu, Z. (2020). Development and validation of a metastasis-related Gene Signature for predicting the Overall Survival in patients with Pancreatic Ductal Adenocarcinoma. J. Cancer *11*, 6299–6318. https://doi.org/10.7150/jca.47629.

20. Zu, F., Liu, P., Wang, H., Zhu, T., Sun, J., Sheng, W., and Tan, X. (2020). Integrated analysis identifies a pathway-related competing endogenous RNA network in the progression of pancreatic cancer. BMC Cancer *20*, 958. https://doi.org/10.1186/s12885-020-07470-4.

21. Krebs, N., Klein, L., Wegwitz, F., Espinet, E., Maurer, H.C., Tu, M., Penz, F., Küffer, S., Xu, X., Bohnenberger, H., et al. (2022). Axon guidance receptor ROBO3 modulates subtype identity and prognosis via AXL-associated inflammatory network in pancreatic cancer. JCI Insight *7*, e154475. https://doi.org/10.1172/jci.insight.154475.

22. Lu, W., Li, N., and Liao, F. (2019). Identification of Key Genes and Pathways in Pancreatic Cancer Gene Expression Profile by Integrative Analysis. Genes *10*, 612. https://doi.org/10.3390/genes10080612.

23. Weissmueller, S., Manchado, E., Saborowski, M., Morris, J.P., 4th, Wagenblast, E., Davis, C.A., Moon, S.H., Pfister, N.T., Tschaharganeh, D.F., Kitzing, T., et al. (2014). Mutant p53 drives pancreatic cancer metastasis through cell-autonomous PDGF receptor beta signaling. Cell *157*, 382–394. https://doi.org/10.1016/j.cell.2014.01.066.

24. Chao, Y.C., Pan, S.H., Yang, S.C., Yu, S.L., Che, T.F., Lin, C.W., Tsai, M.S., Chang, G.C., Wu, C.H., Wu, Y.Y., et al. (2009). Claudin-1 is a metastasis suppressor and correlates with clinical outcome in lung adenocarcinoma. Am. J. Respir. Crit. Care Med. *179*, 123–133. https://doi.org/10.1164/rccm.200803-456OC.

25. Arafat, H., Lazar, M., Salem, K., Chipitsyna, G., Gong, Q., Pan, T.C., Zhang, R.Z., Yeo, C.J., and Chu, M.L. (2011). Tumor-specific expression and alternative splicing of the COL6A3 gene in pancreatic cancer. Surgery *150*, 306–315. https://doi.org/10.1016/j.surg.2011.05.011.

26. Foley, K., Rucki, A.A., Xiao, Q., Zhou, D., Leubner, A., Mo, G., Kleponis, J., Wu, A.A., Sharma, R., Jiang, Q., et al. (2015). Semaphorin 3D autocrine signaling mediates the metastatic role of annexin A2 in pancreatic cancer. Sci Signal *8*, ra77. 10.1126/scisignal.aaa5823.

27. Yong, L.K., Lai, S., Liang, Z., Poteet, E., Chen, F., van Buren, G., Fisher, W., Mo, Q., Chen, C., and Yao, Q. (2016). Overexpression of Semaphorin-3E enhances pancreatic cancer cell growth and associates with poor patient survival. Oncotarget *7*, 87431–87448. https://doi.org/10.18632/oncotarget.13704.

28. Jurcak, N.R., Rucki, A.A., Muth, S., Thompson, E., Sharma, R., Ding, D., Zhu, Q., Eshleman, J.R., Anders, R.A., Jaffee, E.M., et al. (2019). Axon Guidance Molecules Promote Perineural Invasion and Metastasis of Orthotopic Pancreatic Tumors in Mice. Gastroenterology *157*, 838–850.e6.e836. https://doi.org/10.1053/j.gastro.2019.05.065.

29. Kang, N., Gores, G.J., and Shah, V.H. (2011). Hepatic stellate cells: partners in crime for liver metastases? Hepatology *54*, 707–713. https://doi.org/10.1002/hep.24384.

30. Jophlin, L.L., Koutalos, Y., Chen, C., Shah, V., and Rockey, D.C. (2018). Hepatic stellate cells retain retinoid-laden lipid droplets after cellular transdifferentiation into activated myofibroblasts. Am. J. Physiol. Gastrointest. Liver Physiol. *315*, G713–G721. https://doi.org/10.1152/ajpgi.00251.2017.

31. D'Ambrosio, D.N., Walewski, J.L., Clugston, R.D., Berk, P.D., Rippe, R.A., and Blaner, W.S. (2011). Distinct populations of hepatic stellate cells in the mouse liver have different capacities for retinoid and lipid storage. PLoS One *6*, e24993. https://doi.org/10.1371/journal.pone.0024993.

32. Friedman, S.L., Wei, S., and Blaner, W.S. (1993). Retinol release by activated rat hepatic lipocytes: regulation by Kupffer cell-conditioned medium and PDGF. Am. J. Physiol. *264*, G947–G952. https://doi.org/10.1152/ajpgi.1993.264.5.G947.

33. Pattison, J.M., Melo, S.P., Piekos, S.N., Torkelson, J.L., Bashkirova, E., Mumbach, M.R., Rajasingh, C., Zhen, H.H., Li, L., Liaw, E., et al. (2018). Retinoic acid and BMP4 cooperate with p63 to alter chromatin dynamics during surface epithelial commitment. Nat. Genet. *50*, 1658–1665. https://doi.org/10.1038/s41588-018-0263-0.

34. Zheng, L., Xu, M., Xu, J., Wu, K., Fang, Q., Liang, Y., Zhou, S., Cen, D., Ji, L., Han, W., and Cai, X. (2018). ELF3 promotes epithelial-mesenchymal transition by protecting ZEB1 from miR-141-3p-mediated silencing in hepatocellular carcinoma. Cell Death Dis. *9*, 387. https://doi.org/10.1038/s41419-018-0399-y.

35. Wang, W., Friedland, S.C., Guo, B., O'Dell, M.R., Alexander, W.B., Whitney-Miller, C.L., Agostini-Vulaj, D., Huber, A.R., Myers, J.R., Ashton, J.M., et al. (2019). ARID1A, a SWI/SNF subunit, is critical to acinar cell homeostasis and regeneration and is a barrier to transformation and epithelial-mesenchymal transition in the pancreas. Gut *68*, 1245–1258. https://doi.org/10.1136/gutjnl-2017-315541.

36. Sung, P.J., Rama, N., Imbach, J., Fiore, S., Ducarouge, B., Neves, D., Chen, H.W., Bernard, D., Yang, P.C., Bernet, A., et al. (2019). Cancer-Associated Fibroblasts Produce Netrin-1 to Control Cancer Cell Plasticity. Cancer Res. *79*, 3651–3661. https://doi.org/10.1158/0008-5472.CAN-18-2952.

37. Geerts, A., Niki, T., Hellemans, K., De Craemer, D., Van Den Berg, K., Lazou, J.M., Stange, G., Van De Winkel, M., and De Bleser, P. (1998). Purification of rat hepatic stellate cells by side scatter-activated cell sorting. Hepatology *27*, 590–598. https://doi.org/10.1002/hep.510270238.

38. Costa-Silva, B., Aiello, N.M., Ocean, A.J., Singh, S., Zhang, H., Thakur, B.K., Becker, A., Hoshino, A., Mark, M.T., Molina, H., et al. (2015).

Pancreatic cancer exosomes initiate pre-metastatic niche formation in the liver. Nat. Cell Biol. *17*, 816–826. https://doi.org/10.1038/ncb3169.

39. Peinado, H., Alečković, M., Lavotshkin, S., Matei, I., Costa-Silva, B., Moreno-Bueno, G., Hergueta-Redondo, M., Williams, C., García-Santos, G., Ghajar, C., et al. (2012). Melanoma exosomes educate bone marrow progenitor cells toward a pro-metastatic phenotype through MET. Nat. Med. *18*, 883–891. https://doi.org/10.1038/nm.2753.
40. Menck, K., Klemm, F., Gross, J.C., Pukrop, T., Wenzel, D., and Binder, C. (2013). Induction and transport of Wnt 5a during macrophage-induced malignant invasion is mediated by two types of extracellular vesicles. Oncotarget *4*, 2057–2066. https://doi.org/10.18632/oncotarget.1336.
41. Thery, C., Amigorena, S., Raposo, G., and Clayton, A. (2006). Isolation and characterization of exosomes from cell culture supernatants and biological fluids. Curr Protoc Cell Biol *Chapter 3*. Unit *3*. https://doi.org/10.1002/0471143030.cb0322s30.
42. Paradisi, A., Maisse, C., Coissieux, M.M., Gadot, N., Lépinasse, F., Delloye-Bourgeois, C., Delcros, J.G., Svrcek, M., Neufert, C., Fléjou, J.F., et al. (2009). Netrin-1 up-regulation in inflammatory bowel diseases is required for colorectal cancer progression. Proc. Natl. Acad. Sci. USA *106*, 17146–17151. https://doi.org/10.1073/pnas.0901767106.
43. Hong, Y., Li, S., Wang, J., and Li, Y. (2018). In vitro inhibition of hepatic stellate cell activation by the autophagy-related lipid droplet protein ATG2A. Sci. Rep. *8*, 9232. https://doi.org/10.1038/s41598-018-27686-6.
44. Li, Y., Liu, F., Ding, F., Chen, P., and Tang, M. (2015). Inhibition of liver fibrosis using vitamin A-coupled liposomes to deliver matrix metalloproteinase-2 siRNA in vitro. Mol. Med. Rep. *12*, 3453–3461. https://doi.org/10.3892/mmr.2015.3842.
45. Murakami, K.i., Kaji, T., Shimono, R., Hayashida, Y., Matsufuji, H., Tsuyama, S., Maezono, R., Kosai, K.i., and Takamatsu, H. (2011). Therapeutic effects of vitamin A on experimental cholestatic rats with hepatic fibrosis. Pediatr. Surg. Int. *27*, 863–870. https://doi.org/10.1007/s00383-011-2853-0.
46. Matsumoto, Y., Irie, F., Inatani, M., Tessier-Lavigne, M., and Yamaguchi, Y. (2007). Netrin-1/DCC signaling in commissural axon guidance requires cell-autonomous expression of heparan sulfate. J. Neurosci. *27*, 4342–4350. https://doi.org/10.1523/JNEUROSCI.0700-07.2007.
47. Grandin, M., Meier, M., Delcros, J.G., Nikodemus, D., Reuten, R., Patel, T.R., Goldschneider, D., Orriss, G., Krahn, N., Boussouar, A., et al. (2016). Structural Decoding of the Netrin-1/UNC5 Interaction and its Therapeutical Implications in Cancers. Cancer Cell *29*, 173–185. https://doi.org/10.1016/j.ccell.2016.01.001.
48. Cassier, P., Eberst, L., Garin, G., Courbebaisse, Y., Terret, C., Robert, M., Frenel, J.S., Depil, S., Delord, J.P., Perol, D., et al. (2019). A first in human, phase I trial of NP137, a first in class antibody targeting Netrin-1, in patients with advanced refractory solid tumors. Annals of Oncology *30*, v159–v193. https://doi.org/10.1093/annonc/mdz244.

STAR★METHODS

KEY RESOURCES TABLE

REAGENT or RESOURCE	SOURCE	IDENTIFIER
Antibodies		
Anti-netrin 1 antibody [EPR5428]	Abcam	ab126729
Human/Mouse ELF3 Antibody	R&D Systems	AF5787
RXRα (D6H10) Rabbit mAb	Cell Signaling	3085S
ELF3 Polyclonal Antibody	Invitrogen	PA5-89261
Normal Rabbit IgG	Cell Signaling	2729P
RARα/Retinoic Acid Receptor α Antibody (C-1)	Santa Cruz Biotechnology	sc-515796
Mouse (G3A1) mAb IgG1 Isotype Control	Cell Signaling	5415S
Anti-Desmin antibody [Y66]	Abcam	ab32362
Smooth muscle actin Polyclonal antibody	ProteinTech	14395-1-AP
Goat anti-Rabbit IgG (H + L) Cross-Adsorbed Secondary Antibody, Alexa Fluor™ 532	Invitrogen	A-11009
Goat anti-Rabbit IgG (H + L) Cross-Adsorbed Secondary Antibody, Alexa Fluor™ 555	Invitrogen	A-21428
Anti-CD9 antibody [EPR2949]	Abcam	ab92726
UNC5B (D9M7Z) Rabbit mAb	Cell Signaling	13851
Purified Mouse Anti-Flotillin-1	BD Biosciences	610820
Cytokeratin 17 Monoclonal Antibody (CK17)	Thermo Fisher	606–540
RARγ1 (D3A4) XP® Rabbit mAb	Cell Signaling	8965S
Anti-Retinoid X Receptor beta/RXRB antibody	Abcam	ab221115
RXRγ Antibody (G-6)	Santa Cruz Biotechnology	sc-514134
Actin Antibody (H-6)	Santa Cruz Biotechnology	sc-376421
Alix (3A9) Mouse mAb	Cell Signaling	2171S
Alexa Fluor® 647 anti-mouse/human CD324 (E-Cadherin) Antibody	Biolegend	147307
Vimentin (D21H3) XP® Rabbit mAb	Cell Signaling	5741S
alpha-Smooth Muscle Actin Antibody (1A4/asm-1) - Azide and BSA Free	Novus Biologicals	NBP2-34522
mAbNtn1	Patrick Mehlan	N/A
Bacterial and virus strains		
Edit-R Mouse Unc5b hEF1a All-in-one Lentiviral sgRNA	Horizon Discovery	VSGM11942-247910466
Edit-R Mouse Elf3 mCMV All-in-one Lentiviral sgRNA	Horizon Discovery	VSGM11942-248070215
Edit-R Mouse Ntn1 Lentiviral sgRNA	Horizon Discovery	VSGM10144-246774776
Biological samples		
BxPC-3	ATCC	CRL-1687
Capan-2	ATCC	HTB-80
PANC1	ATCC	CRL-1469
MIA PaCa-2	ATCC	CRL-1420
C57BL/6 MOUSE PRIMARY HEPATOCYTES - PLATEABLE	Cell Biologics	C57-6224F
C57BL/6 MOUSE PRIMARY LIVER SINUSOIDAL ENDOTHELIAL CELLS	Cell Biologics	C57-6017

(*Continued on next page*)

Continued

REAGENT or RESOURCE	SOURCE	IDENTIFIER
Chemicals, peptides, and recombinant proteins		
Recombinant human Netrin-1 protein	R&D Systems	1109-N1-025
Retinoic acid	Sigma	R2625
9-cis-retinoic acid	Sigma	R4643
UVI-3003	Selleck Chemicals	S2833
Growth factor reduced matrigel	Corning	354230
Permount™ Mounting Medium	Fisher Scientific	SP15-100
Power SYBR™ Green RNA-to-C_T™ *1-Step* Kit	ThermoFisher Scientific	4391178
Xylazine	Rutgers Animal Care	N/A
Ketamine	Rutgers Animal Care	N/A
Buprenorphine	Rutgers Animal Care	N/A
Collagenase type I	Sigma	SCR103
Hyaluronidase	Sigma	385931
DNAse I	Sigma	260913
Pronase	Sigma	PRON-RO
Hematoxylin Counterstain	Vector Laboratories	H-3401-500
Eosin-Y, alcoholic	Fisher Scientific	22-110-637
Clear-Mount	Fisher Scientific	50-335-66
DAB+ Substrate Chromogen System (Dako Omnis)	Agilent	GV82511-2
Critical commercial assays		
Kwiq-Diff kit	Fisher Scientific	99-907-00
Amicon Ultra-4 Ultracel-3K MWCO	Fisher Scientific	UFC800324
Analytical Sales & Services 1k MWCO Filters with 2mL Receiver Tubes	Fisher Scientific	50-646-345
RNeasy kit	Qiagen	74106
SimpleChIP Plus Sonication Chromatin IP Kit	Cell Signaling	56383
Alexa Fluor® 647 Conjugation Kit (Fast) - Lightning-Link®	Abcam	ab269823
Amicon Ultra-15 centrifugal filter (30K)	Fisher Scientific	UFC903024
0.4 μm Immunobeads for Overall Exosome Isolation (Mouse Cell Media)	Novus Biologicals	NBP2-49833
Cell Counting Kit-8	Dojindo	CK04-11
Lipofectamine 3000	Thermo Fisher Scientific	L3000008
Mouse Ntn1 Taqman Probe	Thermo Fisher Scientific	4331182; Mm00500896_m1
Mouse Elf3 Taqman Probe	Thermo Fisher Scientific	4331182; Mm01295975_m1
Mouse Dcc Taqman Probe	Thermo Fisher Scientific	4331182; Mm00514509_m1
Mouse Unc5a Taqman Probe	Thermo Fisher Scientific	4331182; Mm00462368_m1
Mouse Unc5b Taqman Probe	Thermo Fisher Scientific	4331182; Mm00504054_m1
Mouse Unc5c Taqman Probe	Thermo Fisher Scientific	4331182; Mm00494093_m1
Mouse Unc5d Taqman Probe	Thermo Fisher Scientific	4331182; Mm00467655_m1
Mouse Acta2 Taqman Probe	Thermo Fisher Scientific	4331182; Mm00725412_s1
Mouse Col1a1 Taqman Probe	Thermo Fisher Scientific	4331182; Mm00801666_g1
Mouse Lox Taqman Probe	Thermo Fisher Scientific	4331182; Mm00495386_m1
Mouse Actb Taqman Probe	Thermo Fisher Scientific	4331182; Mm02619580_g1

(*Continued on next page*)

Continued

REAGENT or RESOURCE	SOURCE	IDENTIFIER
Deposited data		
RNAseq from 5 nM ATRA treatment in GEO	https://www.ncbi.nlm.nih.gov/geo/query/acc.cgi?acc=GSE242662	GEO: GSE242662
RNAseq data from Ink4a.1 murine PDAC model	https://doi.org/10.7910/DVN/YZXVA4 https://www.ncbi.nlm.nih.gov/geo/query/acc.cgi?acc=GSE245306	GEO: GSE245306
ATAC-seq data from matched mouse primary and metastatic pancreatic cancer cell lines	https://doi.org/10.7910/DVN/CQPTSI	N/A
Experimental models: Cell lines		
Ink4a.1	Eric Collisson	N/A
MET25	Darren Carpizo	N/A
MET35	Darren Carpizo	N/A
MET36	Darren Carpizo	N/A
MET38	Darren Carpizo	N/A
MET72	Darren Carpizo	N/A
K8483	David Tuveson	N/A
K8484	David Tuveson	N/A
2838c3	Ben Stanger	N/A
6419c5	Ben Stander	N/A
KP2	David Linehan	N/A
A1809	Aram Hezel	N/A
A2031	Aram Hezel	N/A
A2441	Aram Hezel	N/A
Experimental models: Organisms/strains		
Mus musculus:FVB	The Jackson Laboratory	001800
Mus musculus:INK4.1^{syn_Luc}	Darren Carpizo	N/A
Mus musculus: KPC: KRAS$^{G12D/+}$, Trp53$^{R172H/+}$, Pdx-1-Cre	Darren Carpizo	N/A
Oligonucleotides		
ELF3 promoter forward primer for Sybr green detection	ThermoFisher Scientific	CTGACAATCATTAAAC CAGCCA
ELF3 promoter reverse primer for Sybr green detection	ThermoFisher Scientific	CTCTAAATAGAGCAAAG CAGGAG
NTN1 Intron 1 probe primer	ThermoFisher Scientific	FAM-AACCTGGGA/ZEN/ GCCGGAGAAAGAAC-IABkFQ
NTN1 Intron 1 forward primer	ThermoFisher Scientific	AAGAAGAAAGTTAAAGC CAACGG
NTN1 Intron 1 reverse primer	ThermoFisher Scientific	TGCTTTCTCTTTGTCTCTGCT
CRE probe primer	ThermoFisher Scientific	6FAM-AAACATGCTTCATCG TCGGTCCGG-BHQ
CRE forward primer	ThermoFisher Scientific	GCGGTCTGGCAGTAAAAA CTATC
CRE reverse primer	ThermoFisher Scientific	GTGAAACAGCATTGCTGT CACTT
Recombinant DNA		
pCMV6-Entry Mammalian Expression Vector	Origene	PS100001

(*Continued on next page*)

Continued

REAGENT or RESOURCE	SOURCE	IDENTIFIER
ESE1 (ELF3) (NM_004433) Human Tagged ORF Clone	Origene	RC200631
Software and algorithms		
ImageScope software	Leica Biosystems Imaging	N/A
VisioPharm 19 software	VisioPharm	N/A
GraphPad Prism	GraphPad	N/A
QuPath digital pathology analysis software	https://qupath.github.io/	N/A
Integrated Genome Browser	https://bioviz.org/	N/A
FastQC	https://www.bioinformatics.babraham.ac.uk/projects/fastqc/	N/A
Salmon	https://combine-lab.github.io/salmon/getting_started/	N/A
EdgeR	https://bioconductor.org/packages/release/bioc/html/edgeR.html	N/A
R package GAGE	https://bioconductor.org/packages/release/bioc/html/gage.html	N/A
Morpheus	https://software.broadinstitute.org/morpheus/	N/A
ShinyGO 0.77	http://bioinformatics.sdstate.edu/go/	N/A
Other		
Covidien 30-gauge needles	Fisher Scientific	22-557-172
CELOX Rapid Hemostatic Gauze	Fisher Scientific	NC1419211
Ethicon PDS II (Polydioxanone) Suture, Size 5-0, RB-1, 27″	Fisher Scientific	NC1985442
BD Autoclip Wound Closing System	Fisher Scientific	22–275998
Falcon Cell Culture Inserts, 8 μm	Fisher Scientific	08-771-21

Lead contact

Further information and requests for resources and reagents should be directed to the lead contact, Dr. Darren Carpizo (Darren_Carpizo@URMC.Rochester.edu).

Materials availability

This study did not generate new reagents. All materials are available upon request by contacting the lead contact.

Data and code availability

- RNA-seq data from the Ink4a.1 orthotopic model has been deposited in at Dataverse and is publicly available as of the date of publication. DOIs are listed in the key resources table. It also made available in GEO:GSE245306. The RNA-seq data from Ink4a.1 cells treated with 5nM ATRA is also available in GEO:GSE242662. ATAC-seq data has been deposited at Dataverse and is publicly available as of the date of publication. DOIs are listed in the key resources table.
- This paper does not report original code.
- Any additional information required to reanalyze the data reported in this paper is available from the lead contact upon request.

EXPERIMENTAL MODEL AND STUDY PARTICIPANT DETAILS

All animal protocols were approved by the Rutgers Biomedical and Health sciences Animal Care and Use Committee, or the University of Rochester Committee on Animal Resources. Five-to six-week-old male or female FVB mice were purchased from The Jackson Laboratory (Bar Harbor, ME), or bred in-house following established vivarium approved protocols. KPC mice ($Kras^{G12D/+}$, $Trp53^{R172H/+}$,Pdx-1-Cre) were bred following University of Rochester Committee on Animal Resources approved protocols. KPC mice began screening with twice weekly palpation and once weekly abdominal ultrasound to identify pancreas tumors. Upon

identification of mice with tumors greater than 5mm mice were randomized into treatment arms. Mice were monitored daily for survival endpoints. Littermates of the same sex were randomly assigned to experimental groups.

There were no studies directly involving human participants. Human tumor samples were used as part of a TMA. We are not able to provide details such as age, gender or race of the patients that the samples were taken from. This may limit the generalizability of the comparison of Netrin-1 levels in certain PDAC demographic groups.

METHOD DETAILS

Cell lines

Ink4a.1 (gift from Dr. Eric Collisson) is a mouse pancreatic cancer cell line derived from the *p48*^{cre}, *Kras*$^{LSL\_G12D}$, p16$^{-/-}$/*p19*$^{-/-}$ mouse model (Bardeesy et al., 2006). The cell lines MET25, MET35, MET36, MET38 and MET72 were derived from Ink4a.1 as described in Figure 1. K8483 and K8484 are mouse pancreatic cancer cell lines derived from Pdx-1-Cre, *Kras*$^{LSL\_G12D}$, Trp53$^{R172/H/+}$animals, and were a gift from Dr. David Tuveson. 2838c3 and 6419c5 are mouse pancreatic cell lines derived from KPC-YFP animals and were a gift from Dr. Ben Stanger. KP2 is a mouse pancreatic cell line derived from KPC mice and was a gift from Dr. David Linehan. BXPC3, CAPAN2, PANC1 and MIAPACA-2 are human pancreatic cell lines that were purchased from ATCC. A1809, A2031 and A2441 are mouse pancreatic cancer cell lines derived from Ptf1a-Cre; LSL-Kras^{G12D}; Arid1a$^{f/f}$ (KPCA) mice from Dr. Aram Hezel. A knockout of UNC5B was generated in the MET38 cell line by CRISPR-Cas9, using the Edit-R lentivirus VSGM11942-247910466 (Horizon Discovery). All copies of Unc5b were completely removed, as confirmed by Western blot and by DNA sequence analysis near the gRNA target site. A knockdown of Elf3 was generated in the MET38 cell line by CRISPR-Cas9, using the Edit-R lentivirus VSGM11942-248070215 (Horizon Discovery). This reduced but did not remove Elf3 expression, as judged by Western blot. A knockdown of Ntn1 was generated in the MET38 cell line by CRISPR-Cas9, using the Edit-R lentivirus VSGM10144-246774776 (Horizon Discovery). Isolated mouse hepatocytes (C57-6224F) and sinusoidal endothelial cells (C57-6017) were purchased from Cell Biologics and were cultured as recommended by the manufacturer. To treat INK4A cells, conditioned medium from 72-h cultures of hepatocytes and sinusoidal endothelial cells were added in equal volume to DMEM/10% FBS. For proliferation analysis, cells were grown in 96 well plates and assayed at various time using CCK8 solution (Dojindo).

Knockdown and overexpression experiments

Lipofectamine 3000 (Lifetechnologies) was used to transfect INK4A.1 cells with either pCMV6 control vector or with pCMV6-ELF3 (Origene #RC200631). RNA was harvested from transfected cells after 72 h siRNAs were purchased from Horizon Discovery. MIAPACA2 cells were treated with On-TargetPlus SmartPool directed against human ELF3 (L-016080–00-0005), or with On-TargetPlus non-targeting pool (D-001810-10-05). RNAIMAX was used as a transfection reagent. 72 h after transfection, RNA was collected using RNAeasy columns (Qiagen).

Drug treatments

All *trans* retinoic acid (ATRA or RA) and 9-cis retinoic acid (9RA) were purchased from Sigma and resuspended in ethanol. Cells were treated with 1–10 μM of various retinoids at various times and harvested for protein or RNA analysis. To inhibit RXR, 10 μM UVI 3003 (SelleckChem) was used to pretreat cells for 1 h prior to addition of retinoic acids for 24 h. Cells were then harvested for Western blotting analysis.

Migration, invasion, and 3D tumor spheroid sprouting assays

Cells were plated a day prior to overnight starvation in medium containing 0.1% FBS (serum starvation medium, SSM). The next day, 100,000 cells in serum starvation medium were placed in the top of a transwell (8 μm filter, Falcon, 353097), with the bottom chamber containing either SSM, SSM+ 150 ng/mL recombinant human Netrin-1 in PBS/0.2% BSA (R&D Systems, 1109-N1-025), or medium +10% FBS. For invasion assays, transwells were coated with 1 mg/mL growth factor reduced matrigel (Corning) and allowed to solidify 1 h at 37°C prior to loading cells into the chamber. Cells were allowed to migrate/invade for 24 h. Transwells were removed and cells fixed and stained using Diff-Qwik (FisherSci) per the manufacturer's protocol. After 3x PBS washing of transwells, a pre-wetted q-tip was used to remove cells from the upper part of the filter, while the bottom, where cells had migrated through, were not disturbed. The filter was removed from the transwell using a razorblade and laid cell-side down and mounted with a glass coverslip in permount on a glass slide. Slides were cured overnight at room temperature and images taken with the light microscope at 100X. Cells were quantitated per 100X field (n = 10 fields). For the sprouting assay, a single cell suspension in 1:1 matrigel/medium was plated at low density (1000–5000 cells/well of 96-well plate) onto a hardened bed of matrigel and allowed to grow for 7–14 days. Cells were re-fed in complete medium +2% matrigel every 3 days.

ATAC-seq analysis

Cells were harvested and frozen in culture medium containing 5% DMSO. Frozen cells were sent to Active Motif to perform the ATAC-seq assay. The cells were then thawed in a 37°C water bath, pelleted, washed with cold PBS, and fragmented as previously described (Buenrostro et al., 2013) with some modifications (Corces et al., 2017). Briefly, cell pellets were resuspended in lysis buffer, pelleted, and tagmented using the enzyme and buffer provided in the Nextera Library Prep Kit (Illumina). Tagmented DNA was then

purified using the MinElute PCR purification kit (Qiagen), amplified with 10 cycles of PCR, and purified. Resulting material was quantified using the KAPA Library Quantification Kit for Illumina platforms (KAPA Biosystems) and sequenced with PE42 sequencing on the NextSeq 500 sequencer (Illumina). Analysis of ATAC-seq data was very similar to the analysis of ChIP-Seq data. Reads were aligned to the human genome (hg38) using the BWA algorithm (MEME mode; default settings). Duplicate reads were removed, only reads mapping as matched pairs and only uniquely mapped reads (mapping quality $\geq$ 1) were used for further analysis. Alignments were extended in silico at their 3′-ends to a length of 200 bp and assigned to 32-nt bins along the genome. The resulting histograms (genomic ''signal maps'') were stored in bigWig files. Peaks were identified using the MACS 2.1.0 algorithm at a cutoff of p value 1e-7, without control file, and with the –nomodel option. Peaks that were on the ENCODE blacklist of known false ChIP-Seq peaks were removed. Signal maps and peak locations were used as input data to Active Motifs proprietary analysis program, which creates Excel tables containing detailed information on sample comparison, peak metrics, peak locations, and gene annotations. Data tracks were loaded on the Integrated Genome Browser (Bioviz.org) to visualize chromatin open peaks.

RNA-seq analysis

Ink4a.1 and Met cell lines were profiled using standard RNA-seq completed by Azenta Life Sciences (formally known as Genewiz, South Plainfield, NJ). After quality check of the reads using FastQC (https://www.bioinformatics.babraham.ac.uk/projects/fastqc/). We used Salmon (A) to quantify transcript-level expression and EdgeR (B) to identify genes with significantly differential expression between pairs of conditions based on replicated count data from bulk RNA-seq profiling. The normalized data were applied to R package GAGE (C) for gene-set enrichment and pathway analysis. The p values were corrected for multiple testing using FDR. Heat maps were created using Morpheus from the Broad Institute (https://software.broadinstitute.org/morpheus/). Pathway enrichment was analyzed by ShinyGO 0.77 (http://bioinformatics.sdstate.edu/go/).

Size exclusion chromatography

Ink4a.1 cells were plated at a density of 30,000 cells/well of a 12-well plate. Prior to treatment, medium was aspirated and the cells were washed with 1X PBS. A control well of Ink4a.1 was maintained in RPMI+10% FBS. Pooled HSC conditioned medium (CM) from HSCs (Day 6) was filtered with a 0.45 μm filter and added directly to Ink4a.1 cells as a positive control. For size exclusion chromatography for treatments, CM was fractionated with an Amicon Ultra-4 Ultracel-3K MWCO or Ultra-cel-1K MWCO filter and centrifuged at 4°C. 200 μL of CM 3K or 1K concentrate was diluted in 400 μL medium and placed in a well of Ink4a.1 cells in order to determine Netrin-1 induction 24 h later.

Identification of retinoid species by LC/MS

The retinoid measurement was performed on a Vanquish Horizon UHPLC system (Thermo Fisher Scientific, Waltham, MA) with a Poroshell 120 EC-C18 column (150 mm × 2.1 mm, 2.7 μm particle size, Agilent InfinityLab, Santa Clara, CA) using a gradient of solvent A (90%:10% H_2O:MeOH with 34.2 mM acetic acid, 1 mM ammonium acetate, pH 9.4), and solvent B (75%:25% IPA:methanol with 34.2 mM acetic acid, 1 mM ammonium acetate, pH 9.4). The gradient was 0 min, 25% B; 2 min, 25% B; 5.5 min, 65% B; 12.5 min, 100% B; 19.5 min, 100% B; 20.0 min, 25% B; 30 min, 25% B. The flow rate was 200 μL/min. Injection volume was 5 μL and column temperature was 55°C. The autosampler temperature was set to 4°C and the injection volume was 5μL. The full scan mass spectrometry analysis was performed on a Thermo Q Exactive PLUS with a HESI source which was set to a spray voltage of −2.7kV under negative mode and 3.5kV under positive mode. The sheath, auxiliary, and sweep gas flow rates of 40, 10, and 2 (arbitrary unit) respectively. The capillary temperature was set to 300°C and aux gas heater was 360°C. The S-lens RF level was 45. The m/z scan range was set to 100 to 1200m/z under positive ionization mode. The AGC target was set to 1e6 and the maximum IT was 200ms. The resolution was set to 140,000.

Antibodies

NTN1 antibody (1:1000; clone EPR5428; cat #ab126729; Abcam) was used for western blotting and immunohistochemistry (IHC). ELF3 antibody (#AF5787) was purchased from R&D Biosystems and used for Western blots. For immunoprecipitation experiments and western blotting, rabbit polyclonal antibodies against RXRα and ELF3 were purchased from Cell Signaling (3085S) and Invitrogen (PA5-89261), respectively, and compared with normal mouse IgG purchased from Cell Signaling (2729P). For chromatin immunoprecipitation experiments and western blotting, mouse monoclonal against RARα was purchased from Santa Cruz Biotechnology (sc-515796) and compared to an isotype control purchased from Cell Signaling (5415). For IHC, desmin antibody was from Abcam (ab32362), smooth muscle actin was from Proteintech (14395-1-AP), and secondary goat anti-rabbit antibodies were purchased from Invitrogen (A-11009 and A-21428). Other antibodies included CD9 (1:2000; clone EPR2949; cat #ab92726; Abcam); Unc5b (1:1000; clone D9M7Z; cat# 13851; Cell Signaling), mouse polyclonal flotillin-1 (1:500; cat #610820; BD Bioscience); CK17; cat# 606-540; Thermo Fisher), RARγ1 (1:500; clone D3A4; cat# 8965, Cell Signaling), RXRβ (1:500; cat# ab221115; Abcam), RXRγ (clone G-6, cat# sc-514134, Santa Cruz Biotechnology, actin (1:5000; clone H-6; cat# sc-376421; Santa Cruz), and Alix (1:1000; clone 3A9; cat # 2171; Cell Signaling).

Quantitative PCR analysis

Cells were prepared for RNA extraction using the RNAeasy kit (Qiagen). RNA was converted into cDNA using Reverse Transcription Reagents (LifeTechnologies). qPCR assays for Ntn1, Elf3, Dcc, Unc5a, Unc5b, Unc5c, Unc5d, Acta2, Col1a1, Lox, and ActB were

purchased from Life Technologies. RNA was assayed using an Applied Biosystems 7500 Real-Time PCR System. Beta-actin was used as a normalizing control.

Promoter analysis

Chromatin immunoprecipitation experiments were performed using a SimpleChip Plus Sonication kit from Cell Signaling Technology. INK4a cells were treated for 7hr or 19hr treatment with 10 μM ATRA then formaldehyde crosslinked chromatin was generated as recommended by the manufacturer. Quantitative PCR was performed using a 7500 Real Time machine from Applied Biosystems, and QPCR assays were designed and synthesized by Integrated DNA Technologies. PCR amplification of the ELF3 promoter was detected in real time using SYBR Green reagents (Thermofisher) and oligonucleotides 5′CTGACAATCATTAAACCAGCCA 3′ and 5′CTCTAAATAGAGCAAAGCAGGAG 3'. PCR amplification of NTN1 Intron 1 was detected in real time using the probe oligonucleotide 5′FAM-AACCTGGGA/ZEN/GCCGGAGAAAGAAC-IABkFQ-3′ and outside primers 5′AAGAAGAAAGTTAAAGCCAACGG 3′ and 5′TGCTTTCTCTTTGTCTCTGCT-3'.

Flow cytometry

Mouse cell lines were treated for seven days either with DMSO, 10 μM ATRA or 67 μM ATRA. Cells were then gently trypsinized, washed twice in PBS, and resuspended in PBS/0.5% bovine serum albumin. Half of the cells were stained with a fluorescently labeled antibody against native mouse E-cadherin (Biolegend #147307), while the remaining cells were fixed and permeabilized before being stained with an antibody against mouse vimentin (Cell Signaling Technologies #5741S) that had been labeled with AF647 using a Lightning-Link kit (Abcam #ab269823). For flow cytometry using single cell suspensions, fixed and permeabilized single cell liver suspensions were stained for alpha-Smooth-Muscle-Actin (Novus Biologicals, 1A4/asm-1), as well as DAPI prior to imaging. An 18-color LSR Fortessa (nicknamed "Dr Teeth") was used for flow cytometry analysis.

Quantitation of disseminated tumor cells by cre qPCR

Orthotopic pancreatic tumors were generated by injecting FVB mice with 100 cells of Met38 or Met38 NTNKO cell lines in Matrigel. After three weeks, mice were euthanized and genomic DNA was isolated from the entire liver. Quantitation of disseminated tumor cells was performed by qPCR analysis for the presence of cre DNA, which was specific to the cell line and not to the mouse line. The cre probe sequence was 5′-6FAM-AAACATGCTTCATCGTCGGTCCGG-BHQ-3′ and outside primer sequences were 5′GCGGTCTGGCAGTAAAAACTATC-3′ and 5′GTGAAACAGCATTGCTGTCACTT-3'.

Extracellular vesicle isolation by immunobead precipitation

Ink4a.1 and Met38 cells were grown to 80% confluence on 10cm dishes before being washed in PBS and placed in serum free medium for 24 h. The conditioned medium was then collected and centrifuged first at 500g for 10 min, then 1000g for 10 min to remove any cells and debris. This clarified conditioned medium was then filtered using a 20μM syringe-tip filter and concentrated 1:60 using a centrifugal filter unit (Amicon Ultra-15, Merk-Millipore). Extracellular vesicles were isolated from conditioned medium concentrates per manufacturer instructions using 0.4 μm immunobeads for overall exosome isolation kit (Novus biologicals, cat: NBP2-49833). Sizing of EVs was evaluated by transmission electron microscopy by the Department of Pathology's Core Imaging Laboratory at Rutgers University.

EVs isolation by ultracentrifugation

For EVs isolation, cells were seeded in 150 cm^2 dishes at 8 million cells/plate following a 12h attachment period, were washed three times with PBS before supplying 10 mL of serum free medium to prevent contamination from serum-derived EVs. After 72h conditioned medium was collected and EVs were purified: conditioned medium was centrifuged at 2500g for 30 min at 4°C to remove cells and debris. The remaining supernatant was ultracentrifuged at 100 000g for 1h at 4°C to recover EVs.

Animal studies

All animal protocols were approved by the Rutgers Biomedical and Health sciences Animal Care and Use Committee, or the University of Rochester Committee on Animal Resources. Five-to six-week-old female FVB mice were purchased from The Jackson Laboratory (Bar Harbor, ME), or bred in-house following established vivarium approved protocols. For orthotopic studies, 100 Ink4a.1 luc/mcherry pancreatic cells in a mixture of 50% matrigel/50% DMEM +10% FBS were injected into the tail of the pancreas. Buprenorphine and bupivacaine were given for pain management and the mouse was allowed to recover under a heating lamp until ambulatory. For intrasplenic injections, 20-50k cells (see figure legend) in DMEM +10%FBS were injected into the spleen near the hilum. The spleen was then divided distal to the clip and a second clip was placed across the splenic vessels to ensure hemostasis prior to removing the injected hemi-spleen. Buprenorphine and bupivacaine were given for pain management and the mouse was allowed to recover under a heating lamp until ambulatory. Mice were monitored for survival and study endpoints daily post-surgery. KPC mice ($Kras^{G12D/+}$, $Trp53^{R172H/+}$,Pdx-1-Cre) were bred following University of Rochester Committee on Animal Resources approved protocols. KPC mice began screening with twice weekly palpation and once weekly abdominal ultrasound to identify pancreas tumors. Upon identification of mice with tumors greater than 5mm mice were randomized into treatment arms with anti-netrin-1 therapy, or vehicle control and started immediately on twice weekly treatment with 10 mg/kg mAbNtn1, or vehicle control. Mice were monitored daily for survival endpoints.

Liver metastasis assay by portal vein injection

For portal vein injection of pancreatic tumor cells, mice were anesthetized using continuous inhalation of 2–5% isoflurane in O2. The abdominal incision site was sterilized with iodine and ethanol and injected with 1% xylocaine. A dose of at a dose of 0.05–0.1 mg/kg of buprenorphine was administered subcutaneously immediately prior, at the end of operation, and every 4–6 h for 12 h and then every 6–8 h for 3 additional days after surgery. Following laparotomy, the peritoneal cavity was exposed and the loops of intestines exteriorized onto a sterile towel wetted with sterile saline and maintained hydrated with sterile PBS. The portal vein was visualized and injected with a 100 μL of suspension of 5×10^5 PDAC cells suspended in sterile PBS via a 30-gauge needle (Covidien, USA). Successful injection was confirmed by partial blanching of the liver. After removing the needle from the vein, hemostasis was obtained by applying gentle pressure with a Q-tip on a 5 × 5 mm piece of Rapid Hemostatic Gauze (Medtrade Products Ltd.) for 5–10 min. Once no bleeding was seen, the intestines were placed back into the peritoneal cavity, and the peritoneum was closed with resorbable 5-0 PDS II violet suture (Ethicon). Skin was closed using the AutoClip system (Reflex; CellPoint Scientific, Inc.). Following surgery, mice were given buprenorphine and were analyzed after 3 weeks unless indicated otherwise in study designs.

Generation of single-cell suspension of murine livers

freshly harvested liver tissue was digested in 37° DMEM/F12 solution with a combination of collagenase type I (200u/ml), Hyaluronidase (60u/ml), and DAase I (30μg/ml) for 20 min with gentle vortexing. The solution was then strained through a 100μm filter and washed in PBS with 0.5% bovine serum albumin. ACK lysis buffer was added and cells were washed again in PBS with 0.5% bovine serum with DNase I prior counting and dilution to 1000000 cells/ml for antibody staining, and analysis.

Anti-netrin-1 treatment

humanized monoclonal anti-netrin-1 (mAbNtn1) was obtained as a gift from Dr. Patrick Mehlen. mAbNtn1 was delivered via twice weekly intraperitoneal injection at 10 mg/ml concentration diluted in phosphate buffered saline. For murine survival surgery experiments, anti-netrin-1 therapy was initiated 2 days before cell line injection.

Murine hepatic stellate Cell isolation

Hepatic stellate cells were isolated from healthy 9-week-old FVB mice using the protocol previously described (Mederacke et al., 2015). Briefly, mice are anesthetized for non-survival surgery using ketamine and xylazine. A laparotomy incision is made in the abdomen and the inferior vena cava is cannulated using a 26g needle attached to a peristaltic pump. The liver is then perfused *in situ* with pronase-collagenase prior to being removed and further processed *in vitro*. The single cell suspension is then subjected to density gradient centrifugation and stellate cells are collected for experimental use.

H&E staining, immunofluorescence, immunohistochemistry

H&E staining was completed using xylene for deparaffinization and reducing percentages of ethanol for rehydration. Gill's hematoxylin (Vector Labs) and Eosin-Y Alcoholic stain (Richard-Allan Scientific) was used according to manufacturer's instructions. Slides were dehydrated in increasing percentages of ethanol, placed in 3 washes of xylene for 30 s each and mounted using ClearMount (American Mastertech Scientific, Inc). Immuno-staining was completed with deparaffinization and rehydration as above. For IHC on human PDX samples, Netrin-1 expression was measured with indicated antibodies at manufacturer's recommended dilutions and visualized by Liquid DAB chromogen (Dako) and hematoxylin. Slides were scanned (Aperio CS scanner) and regions of interest were outlined manually to enumerate Netrin-1 strong positive cells in ImageScope software (Leica Biosystems Imaging, Inc.). The images were independently validated by a certified pathologist.

Quantitation of liver metastases

Livers were fixed in 4% paraformaldehyde prior to sectioning and H&E staining. Whole slide images were captured at 20× magnification using an Aperio whole slide scanner (Leica Biosystems). Images were then analyzed by pixel classification to identify tumor versus stroma using VisioPharm 19, and QuPath digital pathology analysis software.

QUANTIFICATION AND STATISTICAL ANALYSIS

All experiments were completed in triplicate. Data was analyzed in Excel or GraphPad Prism by students two-tailed t test. Survival statistical analysis was completed in GraphPad by log -rank test. Asterisk identification: *$p < 0.05$, **$p < 0.01$, ***$p < 0.001$, and ****$p < 0.0001$.